

Hierarchical mergers in young, globular and nuclear star clusters: black hole masses and merger rates

MICHELA MAPELLI ^{1,2,3} FILIPPO SANTOLIVU ^{1,2} YANN BOUFFANAIS ^{1,2} MANUEL ARCA SEDDA ⁴
NICOLA GIACOBBO ^{1,2} M. CELESTE ARTALE ⁵ AND ALESSANDRO BALLONE ^{1,2}

¹*Physics and Astronomy Department Galileo Galilei, University of Padova, Vicolo dell'Osservatorio 3, I-35122, Padova, Italy*

²*INFN-Padova, Via Marzolo 8, I-35131 Padova, Italy*

³*INAF-Osservatorio Astronomico di Padova, Vicolo dell'Osservatorio 5, I-35122, Padova, Italy*

⁴*Zentrum für Astronomie der Universität Heidelberg, Astronomisches Rechen-Institut, Mönchhofstrasse 12-14, Heidelberg, D-69120, DE*

⁵*Institut für Astro- und Teilchenphysik, Universität Innsbruck, Technikerstrasse 25/8, A-6020, Innsbruck, Österreich*

(Received; Revised; Accepted)

Submitted to ApJ

ABSTRACT

Hierarchical mergers are one of the distinctive signatures of binary black hole (BBH) formation through dynamical evolution. Here, we present a fast Monte Carlo approach to simulate hierarchical mergers in nuclear star clusters (NSCs), globular clusters (GCs) and young star clusters (YSCs). Hierarchical mergers are orders of magnitude more common in NSCs than they are in both GCs and YSCs, because of the different escape velocity. In our fiducial model, the fraction of hierarchical mergers over all mergers is ~ 0.15 , $\sim 6 \times 10^{-3}$ and $\sim 10^{-4}$ in NSCs, GCs and YSCs, respectively. The mass distribution of hierarchical BBHs strongly depends on the properties of first-generation BBHs, such as their progenitor's metallicity. In our fiducial model, we form black holes (BHs) with masses up to $\sim 10^3 M_\odot$ in NSCs and up to $\sim 10^2 M_\odot$ in both GCs and YSCs. When escape velocities in excess of 100 km s^{-1} are considered, BHs with mass $> 10^3 M_\odot$ are allowed to form in NSCs. Hierarchical mergers lead to the formation of BHs in the pair instability mass gap and intermediate-mass BHs (IMBHs), but only in metal-poor environments. In our fiducial model, at metallicity $Z \sim 0.0002$, the fraction of BBH mergers with primary BH in the pair instability mass gap is $\sim 7 \times 10^{-3}$, 3×10^{-4} and 5×10^{-6} in NSCs, GCs and YSCs, respectively. In metal-poor NSCs, the fraction of BBH mergers with primary mass in the IMBH regime is $\sim 5 \times 10^{-4}$. **The local BBH merger rate in our models ranges from ~ 10 to $\sim 60 \text{ Gpc}^{-3} \text{ yr}^{-1}$; hierarchical BBHs in NSCs account for $\sim 10^{-2} - 0.2 \text{ Gpc}^{-3} \text{ yr}^{-1}$, with a strong upper limit of $\sim 10 \text{ Gpc}^{-3} \text{ yr}^{-1}$.**

Keywords: Astrophysical black holes – Intermediate-mass black holes – Gravitational waves – Star clusters

1. INTRODUCTION

The past four years have witnessed the first two observing runs of the Advanced LIGO and Virgo gravitational-wave (GW) interferometers (Acernese et al. 2015; Aasi et al. 2015), leading to the detection of ten binary black holes (BBHs) and one binary neutron star (BNS) merger (Abbott et al. 2016; Abbott et al.

2016a,b, 2017, 2019a,b). Based on the results of independent pipelines, Zackay et al. (2019), Venumadhav et al. (2020) and Nitz et al. (2020) claimed several additional GW candidates, while Udall et al. (2019) analysed a marginal trigger, which, if interpreted as a BBH coalescence, is a possible intermediate-mass black hole (IMBH) merger remnant.

The third run of the Advanced LIGO and Virgo was recently completed and resulted in more than 50 public

detection candidates¹. Among them, the LIGO-Virgo collaboration (LVC) has already reported a second BNS merger (GW190425, Abbott et al. 2020a), the first BBH event with significantly unequal masses (GW190412, Abbott et al. 2020b), and GW190814, which might be the first black hole – neutron star merger (Abbott et al. 2020c). This growing sample represents a “Rosetta stone” to investigate the formation of binary compact objects.

Several channels can lead to the formation of BBHs: pairing of primordial black holes (e.g. Carr & Hawking 1974; Carr et al. 2016; Bird et al. 2016), binary star evolution through common envelope (e.g. Tutukov & Yungelson 1973; Bethe & Brown 1998; Portegies Zwart & Yungelson 1998; Belczynski et al. 2002; Voss & Tauris 2003; Podsiadlowski et al. 2004; Belczynski et al. 2008; Dominik et al. 2012, 2013; Mennekens & Vanbeveren 2014; Belczynski et al. 2016a; Eldridge & Stanway 2016; Stevenson et al. 2017; Mapelli et al. 2017; Mapelli & Giacobbo 2018; Giacobbo et al. 2018; Giacobbo & Mapelli 2018; Klencki et al. 2018; Kruckow et al. 2018; Spera et al. 2019; Mapelli et al. 2019; Neijssel et al. 2019; Eldridge et al. 2019; Tang et al. 2019) or via homogeneous mixing (e.g. Marchant et al. 2016; de Mink & Mandel 2016; Mandel & de Mink 2016; du Buisson et al. 2020), dynamical processes in triples (e.g. Antonini et al. 2016, 2017; Arca-Sedda et al. 2018; Fragione & Loeb 2019; Fragione & Silk 2020), young/open star clusters (YSCs, e.g. Banerjee et al. 2010; Ziosi et al. 2014; Mapelli 2016; Askar et al. 2017; Banerjee 2017, 2018, 2020; Di Carlo et al. 2019a,b; Kumamoto et al. 2019, 2020), globular clusters (GCs, e.g. Portegies Zwart & McMillan 2000; Downing et al. 2010; Rodriguez et al. 2015, 2016, 2018; Samsing et al. 2014; Samsing 2018; Fragione & Kocsis 2018; Zevin et al. 2019; Antonini & Gieles 2020), nuclear star clusters (NSCs, e.g. O’Leary et al. 2009; Miller & Lauburg 2009; Antonini & Rasio 2016; Petrovich & Antonini 2017; Rasskazov & Kocsis 2019; Arca-Sedda & Gualandris 2018; Arca Sedda & Benacquista 2019; Arca Sedda et al. 2020; Arca Sedda 2020) and AGN disks (e.g. McKernan et al. 2012, 2018; Bartos et al. 2017; Stone et al. 2017; Yang et al. 2019; Tagawa et al. 2019).

One of the distinctive signatures of the dynamical scenario is the formation of hierarchical mergers, i.e. repeated mergers of stellar-origin black holes (BHs) that build up more massive ones (Miller & Hamilton 2002; Fishbach et al. 2017; Gerosa & Berti 2017; Doctor et al. 2020). This process is possible only in dense star clusters, where the merger remnant, which is initially a

single BH, can acquire a companion by dynamical exchanges (Hills & Fullerton 1980). The main obstacle to the formation of second-generation (2g) BHs via hierarchical mergers is the high relativistic kick that the merger remnant receives at birth, because of radiation of linear momentum through beamed GW emission (e.g. Fitchett 1983; Favata et al. 2004; Campanelli et al. 2007; Lousto & Zlochower 2011). This kick can be up to several thousand km s^{-1} and can easily eject the BH remnant from its parent star cluster (Holley-Bockelmann et al. 2008; Moody & Sigurdsson 2009; Fragione et al. 2018; Gerosa & Berti 2019; Arca Sedda et al. 2020). Hence, the interplay between the properties of the host star cluster (e.g. its escape velocity), those of the first-generation (1g) BBH population and the magnitude of the kick decides the maximum mass of a merger remnant in a given environment. This might be used to constrain the formation channels of BBHs. Based on their phenomenological model, Kimball et al. (2020) conclude that none of the 10 BBHs observed by the LVC in the first and second observing runs requires hierarchical mergers, even GW170729. By focusing on GCs, Kimball et al. (2020) find that the median merger rates of 1g+2g and 2g+2g binaries² relative to 1g+1g binaries are $\approx 2.5 \times 10^{-3}$ and $\approx 3.1 \times 10^{-6}$.

The spins of 1g BHs are one of the critical ingredients, because relativistic kicks are sensitive to spin magnitudes and orientation (e.g. Lousto et al. 2012; Maggiore 2018). In the zero-spin assumption, more than 10% of merging BBHs from GCs have components formed from previous mergers, accounting for more than 20% of the mergers from GCs detectable by LIGO–Virgo (Rodríguez et al. 2019).

Due to their high escape velocity ($v_{\text{esc}} \sim 100 \text{ km s}^{-1}$), NSCs are more likely to retain hierarchical mergers than other star clusters (e.g. Antonini & Rasio 2016; Yang et al. 2019; Arca-Sedda & Capuzzo-Dolcetta 2019; Arca Sedda et al. 2020). Antonini et al. (2019) recently found that BH growth becomes substantial for $v_{\text{esc}} > 300 \text{ km s}^{-1}$, leading to the formation of IMBHs (see also Fragione & Silk 2020). Hence, hierarchical mergers can build up IMBHs and also partially fill the pair instability (PI) mass gap between ~ 60 and $\sim 120 M_{\odot}$ (Belczynski et al. 2016b; Woosley 2017; Spera & Mapelli 2017; Farmer et al. 2019; Mapelli et al. 2020; Renzo et al. 2020).

The main challenge of studying hierarchical mergers is the computational cost. It is nearly impossible to inves-

¹ <https://gracedb.ligo.org/>

² Following a common notation, 1g+1g, 1g+2g and 2g+2g binaries are BBHs composed of two 1g BHs, a 1g BH plus a 2g BH, and two 2g BHs, respectively.

tigate the relevant parameter space with hybrid Monte Carlo and/or N-body simulations of star clusters, especially GCs and NSCs. Here, we present a new fast and flexible semi-analytic model to investigate hierarchical mergers in different environments, complementary to dynamical simulations. Our new tool allows us to probe the parameter space (1g masses, spins, delay times, 2g masses, spins and delay times, escape velocity from the parent cluster and kick magnitudes) and to reconstruct the merger rate evolution of each formation channel. With respect to previous work on similar semi-analytic models (Arca Sedda et al. 2020), our new procedure encodes information on the delay time between BBH formation and merger, and can be used to reconstruct the cosmic merger rate density of each considered channel.

2. METHODS

We consider four different environments: i) the field, where hierarchical mergers are not possible, ii) young star clusters (YSCs), which are the main birth site of massive stars in the local Universe (e.g. Portegies Zwart et al. 2010), iii) globular clusters (GCs), and iv) nuclear star clusters (NSCs).

To evaluate the properties of first-generation mergers, we start from catalogs of single and binary BHs obtained with population-synthesis simulations. When the first generation BHs merge, we estimate the relativistic kick v_{kick} and the escape velocity from the parent star cluster v_{esc} . If $v_{\text{kick}} < v_{\text{esc}}$, we assume that the merger remnant remains bound to its parent star cluster and can pair with another BH dynamically. We estimate the mass and spin of the merger remnant and of its new companion, as detailed below. Then, we randomly draw a new delay time between previous and next merger. If the sum of the new delay time and the previous one is shorter than the Hubble time, we repeat the loop for another generation.

2.1. First generation mergers

We take the mass of first generation BHs from our population synthesis simulations. In particular, we used our code MOBSE (Mapelli et al. 2017; Giacobbo et al. 2018; Giacobbo & Mapelli 2018). MOBSE is an upgraded and customized version of BSE (Hurley et al. 2002). In MOBSE, mass loss by stellar winds for massive host stars is modeled as $\dot{M} \propto Z^\beta$, where

$$\beta = \begin{cases} 0.85, & \text{if } \Gamma_e \leq 2/3 \\ 2.45 - 2.4\Gamma_e, & \text{if } 2/3 < \Gamma_e \leq 1 \\ 0.05, & \text{if } \Gamma_e > 1 \end{cases} \quad (1)$$

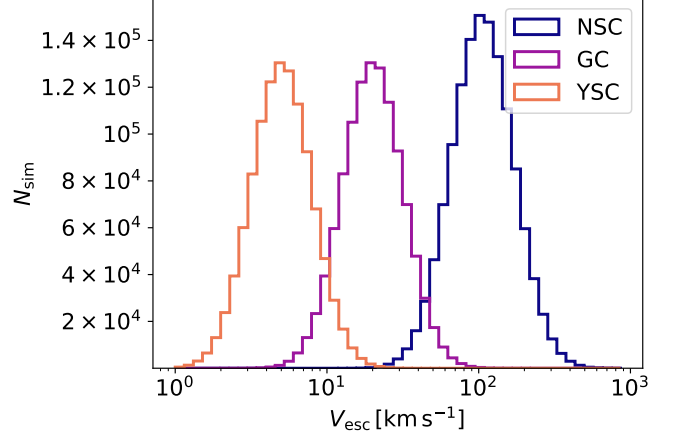


Figure 1. Distribution of escape velocities adopted in the fiducial case. See Section 2.3.

In eq. 1, Γ_e is the Eddington ratio, i.e. the ratio between the luminosity of the star and its Eddington value.

The effect of core-collapse supernovae on the mass of compact objects is described following the delayed model of Fryer et al. (2012). According to this model, stars with final carbon-oxygen mass $m_{\text{CO}} \gtrsim 11 M_\odot$ collapse to a BH directly. The minimum BH mass is $3 M_\odot$. Following Timmes et al. (1996) and Zevin et al. (2020), we compute neutrino mass loss for both neutron stars and BHs as

$$m_\nu = \min \left[\frac{(\sqrt{1 + 0.3 m_{\text{bar}}} - 1)}{0.15}, 0.5 M_\odot \right], \quad (2)$$

where m_{bar} is the baryonic mass of the compact object. The resulting gravitational mass of the compact object is $m_{\text{grav}} = m_{\text{bar}} - m_\nu$.

Stars with helium core mass (at the end of carbon burning) $32 \leq m_{\text{He}} \leq 64$ and $64 \leq m_{\text{He}} \leq 135$ undergo pulsational PI and PI supernovae, respectively (Woosley 2017). Stars that undergo a PI supernova leave no compact remnant, while stars going through pulsational PI become BHs with mass $m_{\text{BH}} = \alpha_P m_{\text{no, PPI}}$, where the possible values of $\alpha_P \leq 1$ are discussed in Mapelli et al. (2020) and $m_{\text{no, PPI}}$ is the BH mass from direct collapse, if pulsational PI is not accounted for. Finally, electron-capture supernovae are included following Giacobbo & Mapelli (2019). For natal kicks, we adopt the prescription $v_k \propto m_{\text{ej}} m_{\text{rem}}^{-1}$, where m_{ej} is the mass of the ejecta and m_{rem} is the mass of the compact remnant (neutron star or BH, Giacobbo & Mapelli 2020).

Binary evolution processes (wind mass transfer, Roche lobe overflow, common envelope, mergers, tidal evolution, GW decays) are implemented as in Hurley et al. (2002), with one significant exception. During Roche

lobe overflow, the accretion rate is calculated as

$$\dot{m}_2 = \begin{cases} f_{\text{MT}} |\dot{m}_1| & \text{if non-degenerate donor} \\ \min(f_{\text{MT}} |\dot{m}_1|, \dot{m}_{\text{Edd}}) & \text{otherwise,} \end{cases} \quad (3)$$

where \dot{m}_1 is the mass loss rate by the donor, \dot{m}_{Edd} is the Eddington accretion rate and $f_{\text{MT}} \in (0, 1]$ is the accretion efficiency. Here, we consider $f_{\text{MT}} = 0.1, 0.5, 1.0$. The original prescriptions by Hurley et al. (2002) are close to $f_{\text{MT}} = 1.0$.

We parametrize common envelope evolution with the parameter α (Hurley et al. 2002). Here, we consider $\alpha = 1, 5, 10$, large values of α meaning that the envelope is easily ejected, without much shrinking of the binary. In its original meaning (Webbink 1984), α is the fraction of orbital energy that is transferred to the envelope during the spiral-in phase. Here, we also consider values of $\alpha > 1$, because the original formalism does not include additional contributions to the energy budget (e.g. Ivanova et al. 2013; Fragos et al. 2019).

Giacobbo et al. (2018) have shown (e.g. their Figure 4) that with these prescriptions for stellar and binary evolution the maximum mass of a single BH can be as high as $m_{\text{BH}} \approx 65 - 70 M_{\odot}$. Such massive BHs come from metal-poor stars ($Z \sim 0.0002$) with initial mass $m_{\text{ZAMS}} \approx 70 - 80 M_{\odot}$, which retain most of their hydrogen envelope at the time of collapse and have sufficiently small helium cores to avoid pulsational PI (Mapelli et al. 2020). However, the maximum mass of a BH merging within a Hubble time as a result of isolated binary evolution is only $m_{\text{BH}} \approx 50 M_{\odot}$ (Giacobbo et al. 2018). This happens because binary stars that are sufficiently tight to merge within a Hubble time by GW emission evolve through mass transfer and common envelope. These processes remove the hydrogen envelope, leading to smaller BH masses. Hence, the resulting BBH cannot have a total mass higher than $m_{\text{TOT}} \approx 100 M_{\odot}$.

In dynamical environments, exchanges and dynamical hardening might allow even more massive BHs to merge, up to total binary masses $m_{\text{TOT}} \approx 130 - 140 M_{\odot}$ (Di Carlo et al. 2019b). For this reason, we consider two different sets of models for first generation masses. In our fiducial model A5F05 (conservative approach), the masses of first generation BBHs are randomly drawn from catalogs of BBH mergers simulated with MOBSE. In this case, the delay time t_{del} between formation and merger of the binary is the same as estimated by the population-synthesis simulation. In the HIGH.MASS model (optimistic approach), the masses of field BBHs are still taken from catalogs of BBH mergers, while the masses of first-generation dynamical BBHs are uniformly drawn from the list of all the BHs formed

with MOBSE, which include both single and binary BHs, both merging and non-merging systems. This ensures that the masses of dynamically formed first-generation BBHs can reach $m_{\text{TOT}} \approx 140 M_{\odot}$, while the maximum total mass of field binaries is $m_{\text{TOT}} \approx 100 M_{\odot}$. In the HIGH.MASS case, we randomly pair the primary and the secondary component and we randomly draw the delay time from a distribution $dN/dt \propto t^{-1}$ between $t_{\text{min}} = 10^7$ yr and $t_{\text{max}} = 1.4 \times 10^{10}$ yr (Dominik et al. 2012; Di Carlo et al. 2019b).

We define spin magnitudes as $a \equiv \mathcal{S} c / (G m_{\text{BH}}^2)$, where \mathcal{S} is the spin magnitude in physical units, G is the gravity constant, m_{BH} is the BH mass and c is the speed of light. Spin magnitudes of first-generation BHs are randomly drawn from a Maxwellian distribution with fiducial one-dimension root-mean square $\sigma_a = 0.2$ and truncated at $a = 1$. We consider also two extreme cases in which $\sigma_a = 0.01$ (LOW_SPIN model) and $\sigma_a = 0.4$ (HIGH_SPIN model). This is just a toy model because the uncertainties on BH spin magnitudes from stellar evolution and core-collapse SN models are still too large to make predictive statements. Angular momentum transport via the magnetic Tayler instability might be effective and lead to predominantly low spins (e.g. Fuller & Ma 2019; Belczynski et al. 2020), while binary evolution processes can significantly affect the overall picture (Qin et al. 2018, 2019). Our LOW_SPIN case can be interpreted as the result of the Fuller & Ma (2019) spin distribution. Spin directions in dynamical BBHs are isotropically distributed over a sphere (Rodriguez et al. 2016).

Our set of runs is described in Table 1. The initial MOBSE population of each model is obtained running 1.2×10^8 first-generation binary stars with metallicity $Z = 0.02, 0.016, 0.012, 0.008, 0.006, 0.004, 0.002, 0.0016, 0.0012, 0.0008, 0.0004, 0.0002$. The initial mass of the primary is drawn from a Kroupa initial mass function (Kroupa 2001) between 5 and $150 M_{\odot}$. Mass ratios, orbital periods and eccentricities are randomly drawn following the distributions presented in Sana et al. (2012).

2.2. Relativistic kicks

We model the magnitude of relativistic kicks following Lousto et al. (2012):

$$v_{\text{kick}} = \left(v_m^2 + v_{\perp}^2 + 2 v_m v_{\perp} \cos \xi + v_{\parallel}^2 \right)^{1/2}, \quad (4)$$

where

$$v_m = A \eta^2 \frac{(1-q)}{(1+q)} (1 + B \eta)$$

$$v_{\perp} = H \frac{\eta^2}{(1+q)} |a_{1\parallel} - q a_{2\parallel}|$$

Table 1. Main properties of the runs presented in this paper

Run Name	BH Masses	α	f_{MT}	t_{del}	σ_a	m_2	t_{del}	t_{min} [Myr]	$\log_{10}(v_{\text{esc}}/\text{km s}^{-1})$
	1g	1g	1g	1g	1g	Ng	Ng	Ng	NSC, GC, YSC
Fiducial, A5F05	BBHs	5.0	0.5	MOBSE	0.2	uniform	t^{-1}	10	$2 \pm 0.2, 1.3 \pm 0.2, 0.7 \pm 0.2$
A5F01	BBHs	5.0	0.1	MOBSE	0.2	uniform	t^{-1}	10	$2 \pm 0.2, 1.3 \pm 0.2, 0.7 \pm 0.2$
A5F1	BBHs	5.0	1.0	MOBSE	0.2	uniform	t^{-1}	10	$2 \pm 0.2, 1.3 \pm 0.2, 0.7 \pm 0.2$
A1F01	BBHs	1.0	0.1	MOBSE	0.2	uniform	t^{-1}	10	$2 \pm 0.2, 1.3 \pm 0.2, 0.7 \pm 0.2$
A1F05	BBHs	1.0	0.5	MOBSE	0.2	uniform	t^{-1}	10	$2 \pm 0.2, 1.3 \pm 0.2, 0.7 \pm 0.2$
A1F1	BBHs	1.0	1.0	MOBSE	0.2	uniform	t^{-1}	10	$2 \pm 0.2, 1.3 \pm 0.2, 0.7 \pm 0.2$
A10F01	BBHs	10.0	0.1	MOBSE	0.2	uniform	t^{-1}	10	$2 \pm 0.2, 1.3 \pm 0.2, 0.7 \pm 0.2$
A10F05	BBHs	10.0	0.5	MOBSE	0.2	uniform	t^{-1}	10	$2 \pm 0.2, 1.3 \pm 0.2, 0.7 \pm 0.2$
A10F1	BBHs	10.0	1.0	MOBSE	0.2	uniform	t^{-1}	10	$2 \pm 0.2, 1.3 \pm 0.2, 0.7 \pm 0.2$
HIGH_MASS	BHs	—	—	t^{-1}	0.2	uniform	t^{-1}	10	$2 \pm 0.2, 1.3 \pm 0.2, 0.7 \pm 0.2$
SMALL_M2	BBHs	5.0	0.5	MOBSE	0.2	MOBSE	t^{-1}	10	$2 \pm 0.1, 1.3 \pm 0.2, 0.7 \pm 0.1$
LOW_SPIN	BBHs	5.0	0.5	MOBSE	0.01	uniform	t^{-1}	10	$2 \pm 0.2, 1.3 \pm 0.2, 0.7 \pm 0.2$
HIGH_SPIN	BBHs	5.0	0.5	MOBSE	0.4	uniform	t^{-1}	10	$2 \pm 0.2, 1.3 \pm 0.2, 0.7 \pm 0.2$
SHORT_DELAY	BBHs	5.0	0.5	MOBSE	0.2	uniform	t^{-1}	0.1	$2 \pm 0.2, 1.3 \pm 0.2, 0.7 \pm 0.2$
LONG_DELAY	BBHs	5.0	0.5	MOBSE	0.2	uniform	t^{-1}	100	$2 \pm 0.2, 1.3 \pm 0.2, 0.7 \pm 0.2$
BROAD_VESC	BBHs	5.0	0.5	MOBSE	0.2	uniform	t^{-1}	10	$2 \pm 0.3, 1.3 \pm 0.3, 0.7 \pm 0.3$
NARROW_VESC	BBHs	5.0	0.5	MOBSE	0.2	uniform	t^{-1}	10	$2 \pm 0.1, 1.3 \pm 0.1, 0.7 \pm 0.1$

NOTE—Column 1: Name of the model. Column 2: mass of first generation (1g) BHs; ‘BBHs’ means that 1g BBHs were taken from catalogs of isolated BBH mergers simulated with MOBSE; ‘BHs’ means that 1g BBHs were taken from catalogs of single and binary BHs simulated with MOBSE and randomly paired (used only in the HIGH_MASS run). Column 3: parameter α of the common envelope for 1g BBHs. Column 4: parameter f_{MT} of accretion efficiency for non-degenerate accretors (eq. 3). Column 5: delay time distribution of 1g BBHs; ‘MOBSE’ indicates that the delay times were taken from catalogs of isolated BBH mergers simulated with MOBSE; ‘ t^{-1} ’ means that delay times were randomly drawn from $dN/dt \propto t^{-1}$ even for 1g BBHs. Column 6: one-dimensional root-mean square associated with the Maxwellian distribution used to extract 1g spin magnitudes; we adopted values $\sigma_a = 0.2$ (fiducial), 0.01 (LOW_SPIN), 0.4 (HIGH_SPIN). Column 7: distribution from which we drew the mass of the secondary in the Ng BBHs; ‘uniform’ means that m_2 is uniformly distributed between $m_{\text{MIN}} = 3 M_{\odot}$ and $m_{\text{MAX}} = m_1$ (fiducial), ‘MOBSE’ means that we randomly selected m_2 from catalogs of BHs simulated with MOBSE (used in the SMALL_M2 run). Column 8: delay time distribution of Ng BBH; ‘ t^{-1} ’ means that delay times were randomly drawn from $dN/dt \propto t^{-1}$. Column 9: t_{min} is the minimum delay time for Ng BBHs. Column 10: mean and standard deviation of the lognormal distribution of escape velocities v_{esc} for NSCs, GCs and YSCs.

$$v_{\parallel} = \frac{16\eta^2}{(1+q)} \left[V_{1,1} + V_A S_{\parallel} + V_B S_{\parallel}^2 + V_C S_{\parallel}^3 \right] \\ |a_{1\perp} - q a_{2\perp}| \cos \phi_{\Delta} - \phi. \quad (5)$$

In the above equations, $q = m_2/m_1$ with $m_2 \leq m_1$, $\eta = q(1+q)^{-2}$, $A = 1.2 \times 10^4 \text{ km s}^{-1}$, $B = -0.93$, $H = 6.9 \times 10^3 \text{ km s}^{-1}$, $(V_{1,1}, V_A, V_B, V_C) = (3678, 2481, 1792, 1506) \text{ km s}^{-1}$, $\xi = 145^\circ$ (Lousto & Zlochower 2009), while \vec{a}_1 and \vec{a}_2 are the spin vectors of the primary and secondary BHs, respectively. Moreover, $a_{1\parallel}$ ($a_{2\parallel}$) is the component of the spin of the primary (secondary) BH parallel to the orbital angular momentum of the binary system, while $a_{1\perp}$ ($a_{2\perp}$) is the component of the spin of the primary (secondary) BH lying in the orbital

plane. S_{\parallel} is the component parallel to the orbital angular momentum of the vector $\vec{S} = 2(\vec{a}_1 + q^2 \vec{a}_2)/(1+q)^2$. Finally, ϕ_{Δ} represents the angle between the direction of the infall at merger (which we randomly draw in the BBH orbital plane) and the in-plane component of $\vec{\Delta} \equiv (m_1 + m_2)^2 (\vec{a}_1 - q \vec{a}_2)/(1+q)$, while ϕ is the phase of the BBH, randomly drawn between 0 and 2π .

2.3. Escape velocities

For each merger, we calculate the relativistic kick magnitude as in eq. 4 and then we compare it with the escape velocity of the host environment v_{esc} . If $v_{\text{kick}} < v_{\text{esc}}$, the remnant is retained in its host envi-

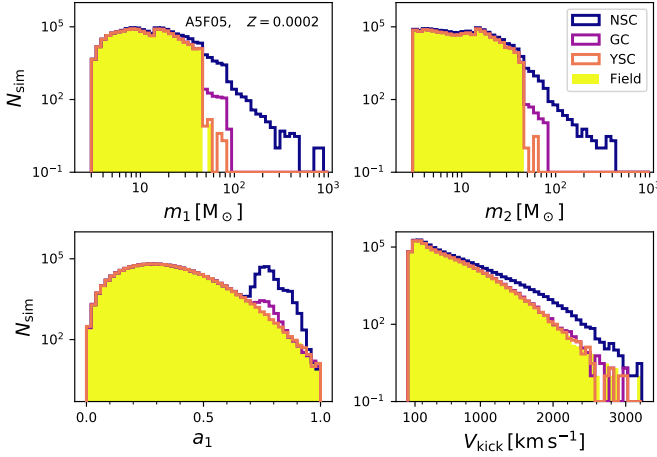


Figure 2. Upper left (right): primary (secondary) mass distribution in the fiducial model A5F05 for $Z = 0.0002$. Lower left (right): primary spin magnitude a_1 (relativistic kick velocity v_{kick}) in the fiducial case for $Z = 0.0002$. The distributions for each channel are drawn from an initial (i.e. zero-age main sequence) stellar population of $1.5 \times 10^{10} M_{\odot}$, assuming a binary fraction $f_{\text{bin}} = 0.5$.

ronment and can undergo another merger. Otherwise, it is ejected and remains a single BH. We randomly draw v_{esc} from a log-normal distribution with median $\langle \log_{10}(v_{\text{esc}}/\text{km s}^{-1}) \rangle = 2.0, 1.3, 0.7$ (standard deviation $\sigma_v = 0.2, 0.2, 0.2$) for NSCs, GCs, and YSCs, respectively (Antonini & Rasio 2016). Figure 1 shows the distribution of escape velocities in our fiducial case. In the next sections, we show what happens if we change these assumptions. Namely, in the BROAD.VESC (NARROW.VESC) model we assume $\sigma_v = 0.3$ (0.1) for NSCs, GCs and YSCs.

2.4. N th generation mass and spin

We model the mass and spin of a merger remnant using the fitting formulas in Jiménez-Forteza et al. (2017) (for quasi-circular non-precessing mergers, see also Rezzolla et al. 2008; Hofmann et al. 2016; Arca Sedda et al. 2020). The final mass is ≈ 0.95 the total mass of the two merging BHs, while the final spin magnitude clusters around $a_f \approx 0.75$.

If the merger remnant is retained, we assume that it eventually pairs with another BH. The mass of the companion is selected in two different ways. To account for the fact that the secondary BH might be either a 1g or a N th generation object, with $N > 1$, we uniformly draw the mass of the secondary m_2 between $m_{\text{MIN}} = 3 M_{\odot}$ and $m_{\text{MAX}} = m_1$ (fiducial model). This assumption favors $Ng - Ng$ mergers with respect to $Ng - 1g$ mergers. To account for cases in which the primary is a N th generation merger (with $N > 1$) and the secondary

is always a first generation BH, we draw the mass of the secondary from the population-synthesis catalogs of 1g BHs (model SMALL_M2).

The spins of the secondary are randomly drawn from a Maxwellian distribution with default one-dimensional root-mean square $\sigma_a = 0.2$. In the LOW_SPIN (HIGH_SPIN) case, $\sigma_a = 0.01$ (0.4). The spin vectors of both the primary and the secondary are isotropically distributed over a sphere. This is a simplification, because we do not distinguish whether the secondary is a Ng or a 1g BH.

Finally, in all models we add a check that the mass of the remnant BH is always less than

$$m_{\text{th}} = 10^{-3} m_{\text{SC}} \approx 10^3 M_{\odot} \left(\frac{v_{\text{esc}}}{100 \text{ km s}^{-1}} \right)^2. \quad (6)$$

This condition is equivalent to assuming that the most massive BH cannot be more massive than the total mass of all BHs in the star cluster, assuming a Kroupa IMF. If a BH hits this mass threshold, it cannot grow any further by hierarchical merger.

2.5. Delay times

For first generation mergers in the fiducial case, the delay times are directly taken from our population-synthesis simulations. For N th generation mergers (where $N = 2$ or more) and for first generation dynamical BBHs in the HIGH_MASS model (see Section 2.1), we randomly draw the delay times according to a distribution uniform in $dN/dt \propto t^{-1}$ (Dominik et al. 2012) and spanning from $t_{\text{min}} = 10^7$ yr to $t_{\text{max}} = 1.4 \times 10^{10}$ yr. This delay time is assumed to be the sum of t_{dyn} and t_{GW} , where t_{dyn} is the time elapsed between the formation of the BH and the dynamical interaction that brings it into a BBH, while t_{GW} is the timescale for BBH coalescence by GW emission.

This is the crudest assumption in our fast procedure, but is supported by N -body simulations of dense YSCs (Di Carlo et al. 2019a,b), which show that dynamical BBH mergers follow a trend $dN/dt \propto t^{-1}$. Antonini et al. (2019) modeled the pairing process in greater detail; they first account for the dynamical friction timescale, i.e. for the time needed for the merger remnant, which is ejected in the outskirts of the star cluster by the relativistic kick, to sink back to the center of the parent cluster by dynamical friction. This is

$$t_{\text{DF}} = 9.5 \text{ Myr} \left(\frac{m_{\text{BH}}}{30 M_{\odot}} \right)^{-1} \left(\frac{M_{\text{SC}}}{10^6 M_{\odot}} \right) \left(\frac{n}{10^6 \text{ pc}^{-3}} \right)^{-1/2}, \quad (7)$$

where M_{SC} and n are the star cluster mass and central number density. After the BH has sunk back to the core of the parent star cluster, it is reasonable to assume that

$Z = 0.0002$

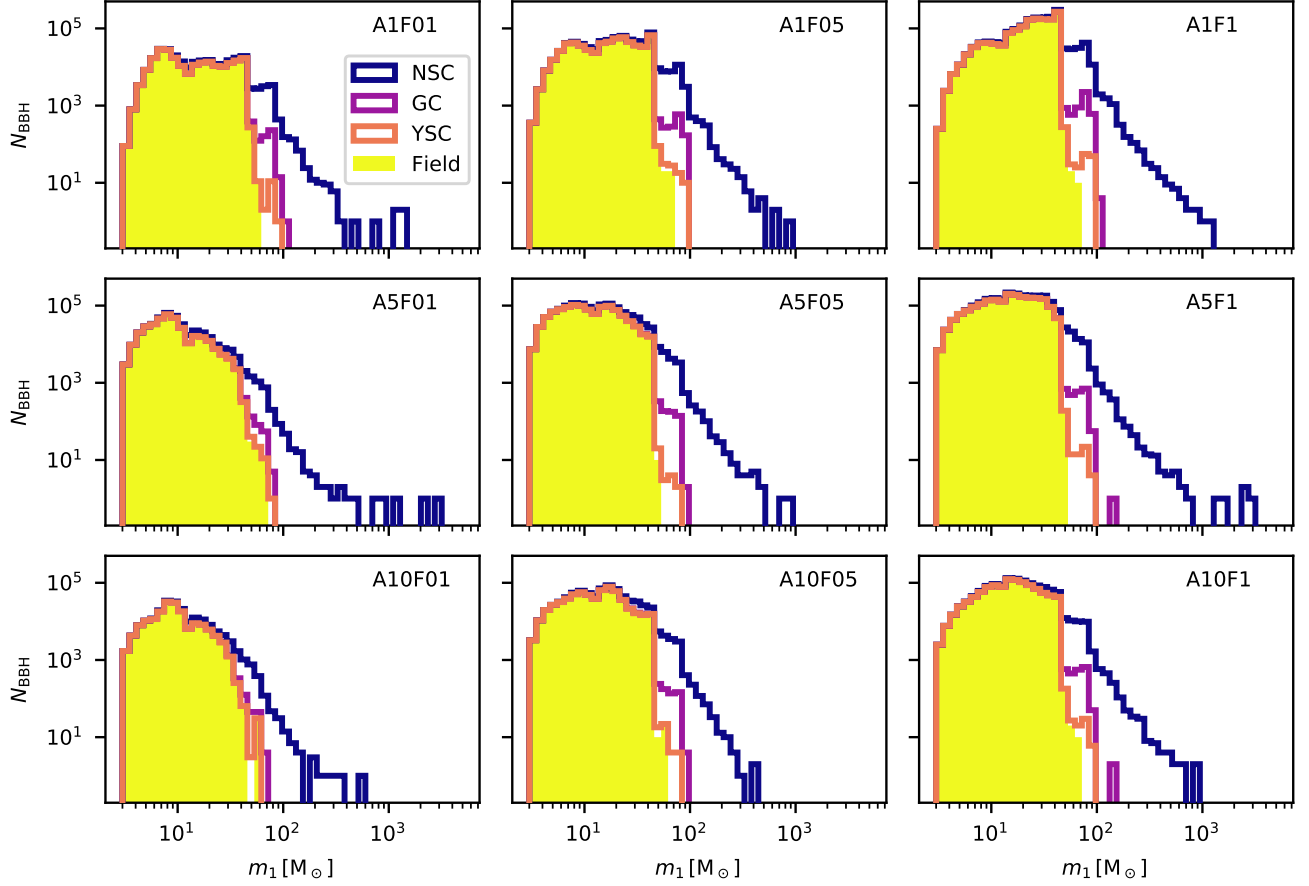


Figure 3. From top to bottom and from left to right: distribution of primary BH masses (m_1), assuming progenitor metallicity $Z = 0.0002$, in the cases A1F01 ($\alpha = 1$, $f_{\text{MT}} = 0.1$), A1F05 ($\alpha = 1$, $f_{\text{MT}} = 0.5$), A1F1 ($\alpha = 1$, $f_{\text{MT}} = 1$), A5F01 ($\alpha = 5$, $f_{\text{MT}} = 0.1$), A5F05 ($\alpha = 5$, $f_{\text{MT}} = 0.5$, fiducial case), A5F1 ($\alpha = 5$, $f_{\text{MT}} = 1$), A10F01 ($\alpha = 10$, $f_{\text{MT}} = 0.1$), A10F05 ($\alpha = 10$, $f_{\text{MT}} = 0.5$), A10F1 ($\alpha = 10$, $f_{\text{MT}} = 1$). The distributions for each channel are drawn from an initial (i.e. zero-age main sequence) stellar population of $1.5 \times 10^{10} M_{\odot}$, assuming a binary fraction $f_{\text{bin}} = 0.5$.

it will pair on a timescale for BBH formation by three-body encounters (Lee 1995):

$$t_{3\text{bb}} = 0.1 \text{ Myr} \left(\frac{n}{10^6 \text{ pc}^{-3}} \right)^{-2} \left(\frac{\sigma_{\text{SC}}}{30 \text{ km s}^{-1}} \right)^9 \left(\frac{m_{\text{BH}}}{30 M_{\odot}} \right)^{-5}, \quad (8)$$

where $\sigma_{\text{SC}} = v_{\text{esc}}/(2\sqrt{3})$ is the velocity dispersion. In both eqs. 7 and 8 we have assumed that the average mass of a star in the star cluster is $1 M_{\odot}$. The dynamical timescale is then $t_{\text{dyn}} = t_{\text{DF}} + t_{3\text{bb}}$. This quantity should be evaluated per each single cluster, but is generally close to our assumption for $t_{\text{min}} = 10$ Myr. Finally, in the LONG_DELAY (SHORT_DELAY) model, we consider $t_{\text{min}} = 100$ (0.1) Myr (Table 1).

2.6. Summary of the models

In Table 1, A5F05 is our fiducial model. Models with name AiFj (with $i = 1, 5, 10$ and $j = 01, 05, 1$) differ from the fiducial model only for the choice of the com-

mon envelope parameter α ($\alpha = 1, 5, 10$ if $i = 1, 5, 10$) and of the accretion efficiency f_{MT} ($f_{\text{MT}} = 0.1, 0.5, 1$ if $j = 01, 05, 1$). The model HIGH_MASS differs from the fiducial model for the choice of the masses of $1g$ BHs and for their delay time distribution. In the model HIGH_MASS, $1g$ BH masses in star clusters are uniformly sampled from all BHs generated with MOBSE (including single BHs), mimicking the impact of dynamical exchanges. Delay times are drawn from $dN/dt \propto t^{-1}$.

The SMALL_M2 model differs from the fiducial model for the masses m_2 of secondary BHs in N_g mergers, which are randomly drawn from first generation BHs. Hence, in this model all BBH mergers occur with a $1g$ secondary BH. In contrast, m_2 is uniformly sampled in $[3M_{\odot}, m_1]$ in all the other models.

The LOW_SPIN and HIGH_SPIN models differ from the fiducial model only for the distribution of spin magnitudes of $1g$ BHs. The one-dimensional root-

$Z = 0.002$

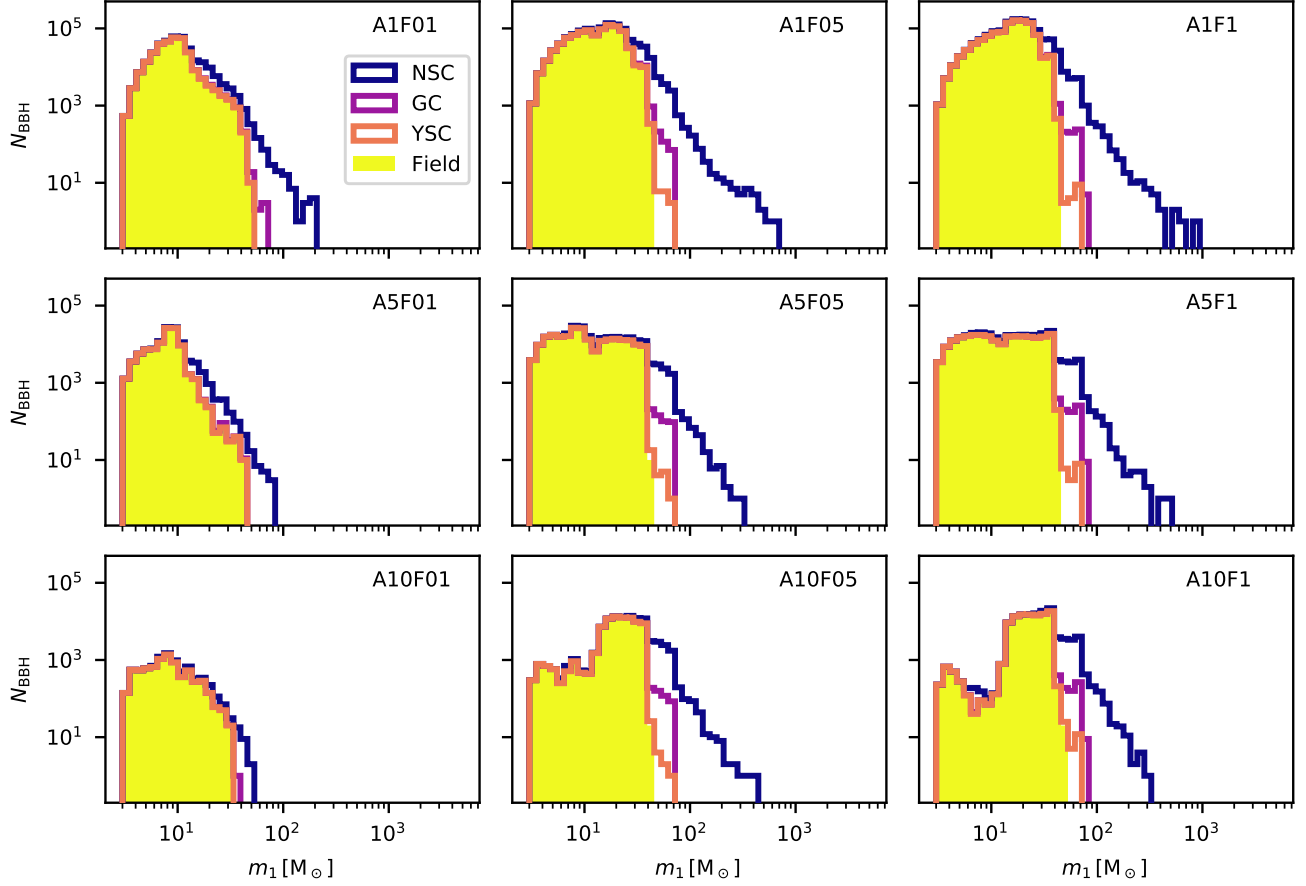


Figure 4. Same as Figure 3 but for progenitor's metallicity $Z = 0.002$.

mean square σ_a is 0.01 and 0.4 in LOW_SPIN and HIGH_SPIN, respectively.

The SHORT_DELAY and LONG_DELAY models differ only for the minimum value of the delay time t_{\min} of N_g mergers, which is 0.1 and 100 Myr, respectively. Finally, the BROAD_VESC and NARROW_VESC models differ from the fiducial case for the standard deviation of the log-normal distribution of v_{esc} , which is 0.3 and 0.1 in the former and in the latter case.

2.7. Merger Rate

We calculate the merger rate by assuming that each channel accounts for a fraction $f_i(t)$ of the star formation rate density at a given look-back time t (where $i = \text{NSC}, \text{GC}, \text{YSC}$ or field).

In our fiducial model, we assume that $f_{\text{GC}}(t)$ is given by

$$f_{\text{GC}}(t) = f_{\text{max,GC}} \exp \left[-\frac{(t - t_{\text{GC}})^2}{2\sigma_t^2} \right], \quad (9)$$

where $f_{\text{max,GC}} = 0.1$, $t_{\text{GC}} = 11.8$ Gyr and $\sigma_t = 2.5$ Gyr. The parameters t_{GC} and σ_t are chosen based on the age

distribution of Galactic GCs (Gratton et al. 1997, 2003; VandenBerg et al. 2013).

NSCs are likely the result of the dynamical assembly of GCs, which sank to the center of the galactic potential well by dynamical friction (Tremaine et al. 1975; Capuzzo-Dolcetta 1993; Capuzzo-Dolcetta & Mocchi 2008; Antonini et al. 2012; Antonini 2013; Arca-Sedda & Capuzzo-Dolcetta 2014; Arca-Sedda et al. 2015), plus some contribution from in situ star formation (Mapelli et al. 2012). Hence, we assume the same functional form for $f_{\text{NSC}}(t)$, with a different normalization:

$$f_{\text{NSC}}(t) = f_{\text{max,NSC}} \exp \left[-\frac{(t - t_{\text{GC}})^2}{2\sigma_t^2} \right], \quad (10)$$

where $f_{\text{max,NSC}} = 0.01$, while t_{GC} and σ_t are the same as in eq. 9. The values of both $f_{\text{max,GC}}$ and $f_{\text{max,NSC}}$ are calibrated to give a mass budget of GCs and NSCs that matches the observed ones at low redshifts (Harris et al. 2013; Neumayer et al. 2020).

$Z = 0.006$

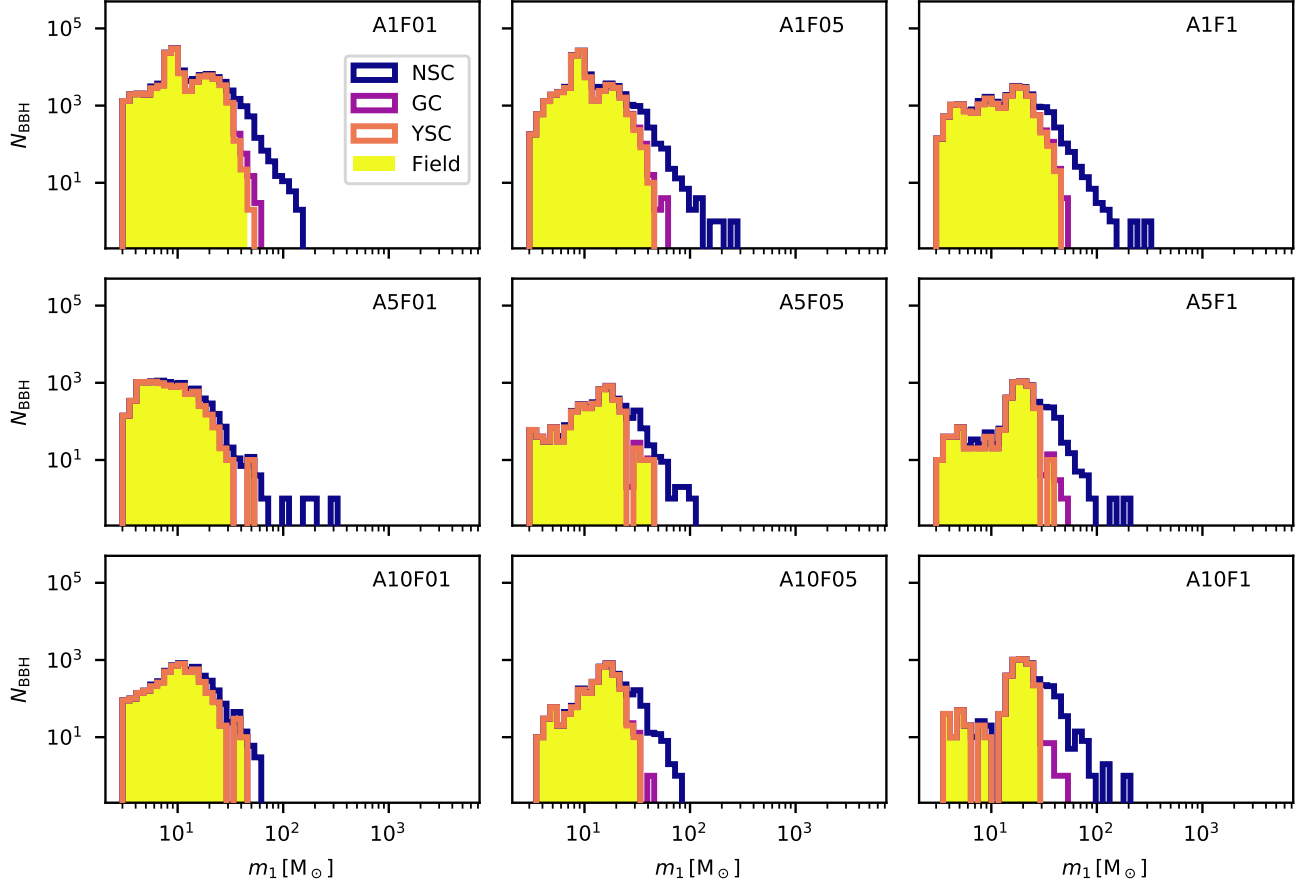


Figure 5. Same as Figure 3 but for progenitor's metallicity $Z = 0.006$.

To keep the fiducial model as simple as possible, we assume

$$f_{\text{YSC}}(t) = \min[0.3, (1 - f_{\text{GC}}(t) - f_{\text{NSC}}(t))]. \quad (11)$$

Finally, we define $f_{\text{field}}(t) = 1 - f_{\text{GC}}(t) - f_{\text{NSC}}(t) - f_{\text{YSC}}(t)$. In the following sections, we briefly discuss the impact of changing the $f_i(t)$ parameters on the merger rate.

The total merger rate for each channel is then evaluated as

$$\mathcal{R}_i(z) = \frac{d}{dt(z)} \int_{z_{\text{max}}}^z f_i(z') \psi(z') \frac{dt(z')}{dz'} dz' \times \int_{Z_{\text{min}}(z')}^{Z_{\text{max}}(z')} \eta(Z) \mathcal{F}(z', z, Z) dZ \quad (12)$$

where $t(z)$ is the look-back time at redshift z , $\psi(z')$ is the cosmic star formation rate density at redshift z' (Madau & Fragos 2017), $f_i(z')$ is the fraction of the total star formation rate that goes into channel $i = \text{NSCs, GCs, YSCs or field}$ at redshift z' , $Z_{\text{min}}(z')$ and $Z_{\text{max}}(z')$ are the minimum and maximum metallicity of stars formed

at redshift z' , $\eta(Z)$ is the merger efficiency at metallicity Z , and $\mathcal{F}(z', z, Z)$ is the fraction of BBHs that form at redshift z' from stars with metallicity Z and merge at redshift z , normalized to all BBHs that form from stars with metallicity Z . To calculate the look-back time we take the cosmological parameters (H_0 , Ω_M and Ω_Λ) from Ade et al. (2016). The maximum considered redshift in equation 12 is $z_{\text{max}} = 15$, which we assume to be the epoch of formation of the first stars. The merger efficiency $\eta(Z)$ is estimated as the number of BBHs that merge within a Hubble time in a coeval population of star with initial mass M_* and metallicity Z , divided by M_* . See Santoliquido et al. (2020) for further details.

3. RESULTS

3.1. Properties of hierarchical mergers

Figure 2 shows the mass of the primary (m_1), the mass of the secondary (m_2), the spin magnitude of the primary (a_1) and the kick velocity (v_{kick}) in the fiducial model (A5F05) for $Z = 0.0002$. The maximum primary and secondary mass strongly depend on the environment: we have 2g BBHs even in YSCs and GCs,

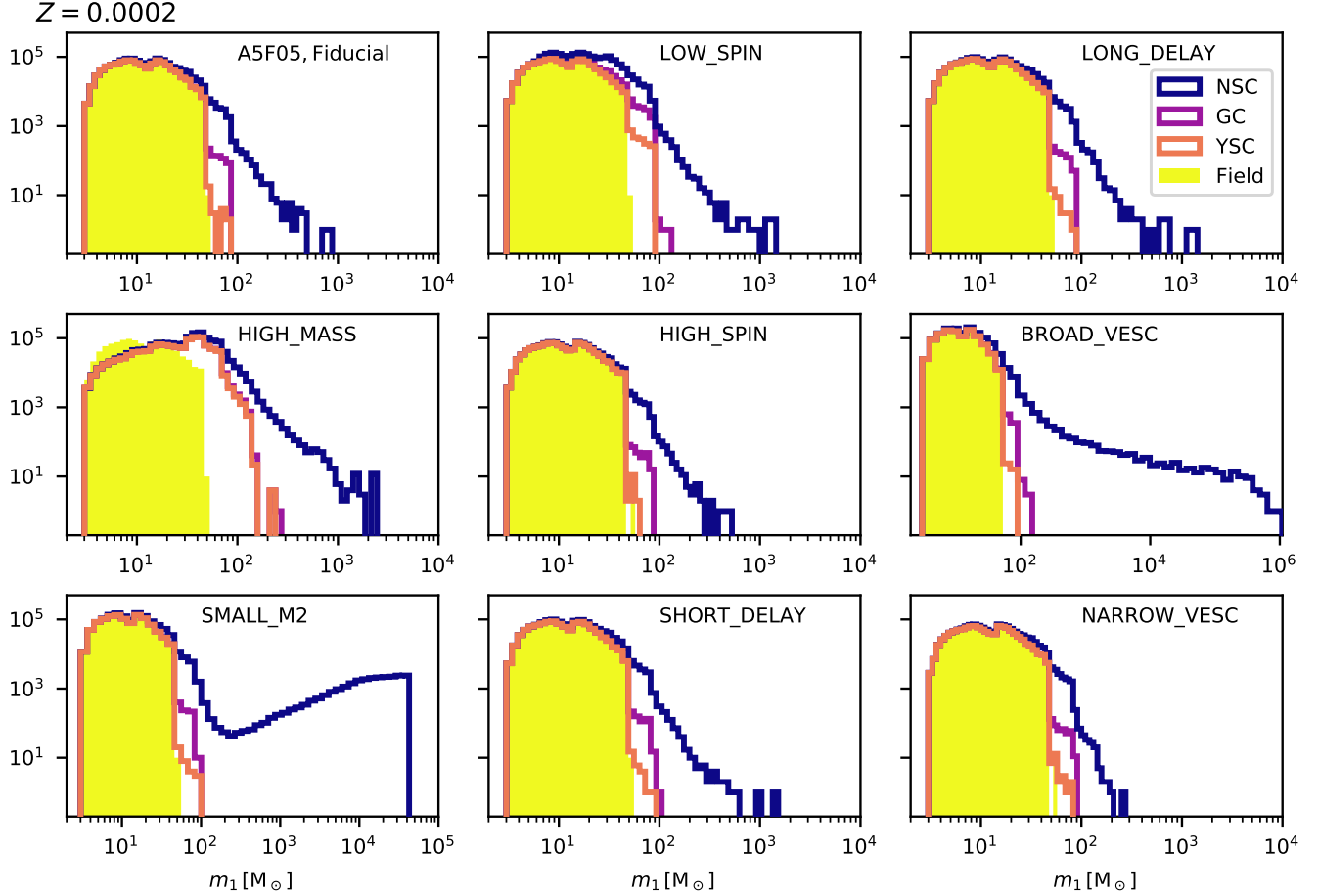


Figure 6. From top to bottom and from left to right: distribution of primary BH masses (m_1), assuming progenitor metallicity $Z = 0.0002$, in the cases A5F05 (fiducial), HIGH_MASS, SMALL_M2, LOW_SPIN, HIGH_SPIN, SHORT_DELAY, LONG_DELAY, BROAD_VESC, NARROW_VESC. The distributions for each channel are drawn from an initial (i.e. zero-age main sequence) stellar population of $1.5 \times 10^{10} M_\odot$, assuming a binary fraction $f_{\text{bin}} = 0.5$.

but NSCs are more effective in producing hierarchical mergers, because of the larger value of v_{esc} . In the fiducial model, the maximum primary mass is $\approx 100 M_\odot$ in YSCs and GCs, while it is close to $\approx 10^3 M_\odot$ in NSCs. The distribution of primary spin magnitudes shows a clear secondary peak at $a_1 \approx 0.7 - 0.8$ in both GCs and NSCs, corresponding to the typical values of N_g merger remnants.

Figures 3, 4 and 5 compare the primary mass distributions that we obtain by varying the values of α and f_{MT} in the first generation of BHs for metallicity $Z = 0.0002, 0.002$ and 0.006 , respectively. By comparing Figures 3, 4 and 5, it is apparent that both the BH mass distribution and the maximum BH mass strongly depend on progenitor’s metallicity, even in hierarchical mergers. At high metallicity ($Z \gtrsim 0.006$), hierarchical mergers can hardly reach masses $\gtrsim 200 M_\odot$. We do not show metallicities $Z > 0.006$ because the maximum mass and the number of hierarchical mergers decrease

dramatically at higher metallicity. Also, the efficiency of common-envelope ejection α and the efficiency of mass accretion f_{MT} significantly affect the mass distribution of N_g BHs. Hence, the mass distribution of $1g$ BBHs, which strongly depends on metallicity, has a crucial impact on the mass distribution of N_g BHs.

In Figure 6, we fix $\alpha = 5$, $f_{\text{MT}} = 0.5$ and $Z = 0.0002$, and we consider the impact of the other main parameters of our model. Drawing the mass of the first generation from the distribution of all $1g$ BHs (instead of considering only $1g$ BBH mergers) shifts the entire distribution of dynamical mergers to higher masses. In the model HIGH_MASS, the most common primary mass of dynamical BBHs is $\sim 30 - 50 M_\odot$, while the primary masses of field BBHs peak at $\sim 10 M_\odot$. The reason is that MOBSE allows the formation of BHs with mass up to $\sim 65 M_\odot$, but small BHs merge more efficiently than the massive ones, because of the interplay between stellar radii, mass transfer and common envelope evo-

lution. If we randomly pair single BHs from MOBSE data, this effect disappears. Hence, the HIGH_MASS model is realistic if dynamical encounters are very effective, and all star cluster BBHs form from dynamical exchanges. Based on direct N -body simulations coupled with MOBSE, Di Carlo et al. (2019b) have shown that BBHs in YSCs behave in an intermediate way between the HIGH_MASS model and our fiducial model. In the HIGH_MASS model, N_g BHs in both GCs and YSCs can reach masses $m_1 \sim 200 M_\odot$, while the maximum mass of N_g BHs in NSCs is $\sim 2000 M_\odot$.

In the SMALL_M2 model, we always draw the secondary mass from the distribution of 1g BHs, which is equivalent to assume that only N_g -1g mergers are possible. Hence, this model differs from the others because of the smaller values of $q = m_2/m_1$ in hierarchical mergers. We observe a peculiar trend of m_1 in the NSC case: values of $m_1 \sim 10^4 M_\odot$ are about one order of magnitude more common than $m_1 \sim 200 M_\odot$. The reason is that relativistic kicks get smaller and smaller if q tends to zero. Hence, the maximum mass of the primary BH in this model is set by the number of hierarchical mergers that can happen within a Hubble time, rather than by the relativistic kicks.

If we compare the LOW_SPIN ($\sigma_a = 0.01$) and the HIGH_SPIN model ($\sigma_a = 0.4$), we see that high mass BHs are more and more suppressed if the spin distribution moves to higher values, because relativistic kicks get stronger. In contrast, we find only a mild difference between the SHORT_DELAY and the LONG_DELAY model, in which we change the minimum delay time t_{\min} .

Finally, the escape velocity has a large impact on hierarchical BH masses, especially for NSCs. BHs with mass up to $\sim 10^6 M_\odot$ form if $\sigma_v = 0.3$ (BROAD_VESC), two orders of magnitude more than if $\sigma_v = 0.2$ (fiducial case, A5F05) and three orders of magnitude more than if $\sigma_v = 0.1$ (NARROW_VESC). This result is consistent with both Antonini et al. (2019) and Fragione & Silk (2020), who report that the maximum BH mass approaches $10^6 M_\odot$ if $v_{\text{esc}} \geq 300 \text{ km s}^{-1}$ are considered. This might be a key ingredient to understand the formation of super-massive BHs and the connection between the mass of the central BH and its parent galaxy mass/central velocity dispersion (Ferrarese & Merritt 2000; Gebhardt et al. 2000).

Figure 7 shows the number of BBHs we simulated per each generation N_g in the case of $Z = 0.0002$ and the maximum primary mass in each generation. We show only NSCs because BHs in GCs and YSCs do not exceed the 5th and the 3rd generation, respectively. The maximum number of generations in NSCs ranges from a few to a few thousands. In the fiducial

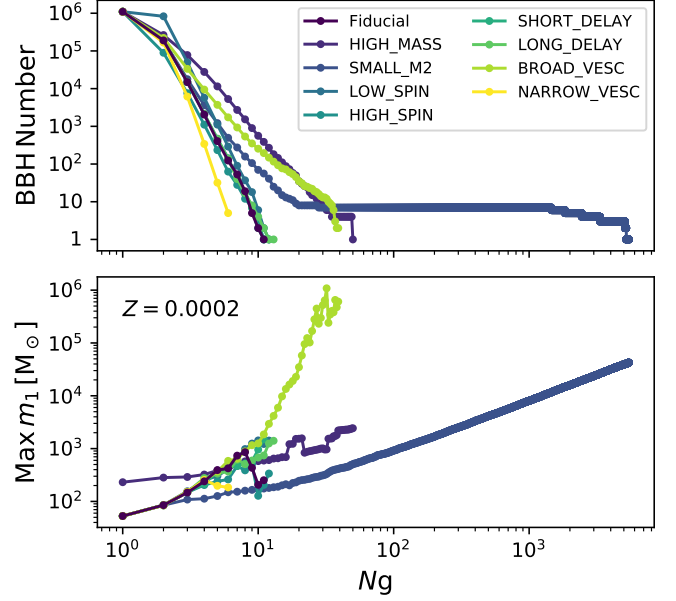


Figure 7. Top: number of BBHs in each generation as a function of the generation number N_g for hierarchical BBHs in NSCs with metallicity $Z = 0.0002$. Bottom: maximum primary BH mass in each generation as a function of the generation number N_g for hierarchical BBHs in NSCs with metallicity $Z = 0.0002$. We show models A5F05 (fiducial), HIGH_MASS, SMALL_M2, LOW_SPIN, HIGH_SPIN, SHORT_DELAY, LONG_DELAY, BROAD_VESC, NARROW_VESC.

case and in most of the other simulations, the maximum number of generations is $N \sim 10$. Only in three cases we obtain a significantly larger number of generations, namely the BROAD_VESC model (≈ 40 generations), the HIGH_MASS model (≈ 50 generations) and the SMALL_M2 model (≈ 5000 generations). The SMALL_M2 case outnumbers all the other models for the number of generations, because of the strong dependence of v_{kick} on q . However, even in this extreme case, the number of N_g mergers with $N \geq 20$ is $\sim 10^5$ times lower than the number of mergers in the first generation.

The top panel of Fig. 8 shows the fraction of N_g BBH mergers with $N > 1$ with respect to all BBH mergers, defined as

$$f_{>1g} = \frac{N_{2g} + N_{3g} + \dots + N_{Ng}}{N_{\text{BBH}}}, \quad (13)$$

where N_{1g} , N_{2g} , N_{3g}, \dots, N_{Ng} is the number of 1g, 2g, 3g, ..., N_g BBH mergers (where N refers to the primary BH only) and N_{BBH} is the total number of BBH mergers summing up all possible generations including the first one. In this figure, $f_{>1g}$ is shown only for NSCs. In the fiducial model and in NSCs, N_g BBH mergers with $N > 1$ are about 16% of all the BBH mergers, with

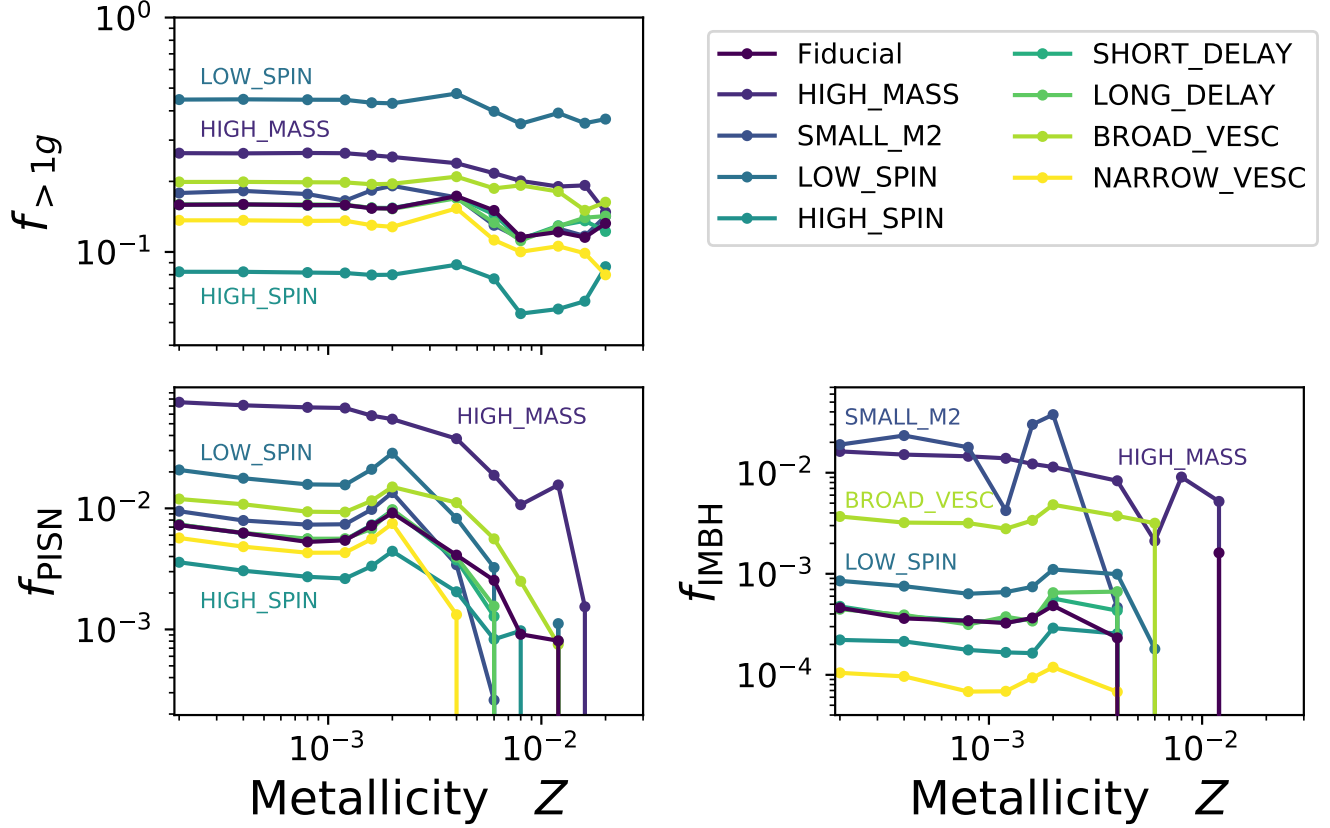


Figure 8. Top: $f_{>1g}$ is the number of N_g BBH mergers with $N > 1$ divided by the total number of BBH mergers. Bottom left: $f_{\text{PI SN}}$ is the number of N_g BBH mergers with a primary mass in the PI mass gap ($m_1 \in [60, 120] M_\odot$), divided by the total number of BBH mergers. Bottom right: f_{IMBH} is the number of N_g BBH mergers with a primary mass in the IMBH regime ($m_1 \geq 100 M_\odot$), divided by the total number of BBH mergers. $f_{>1g}$, $f_{\text{PI SN}}$ and f_{IMBH} refer to NSCs only and are shown as a function of the metallicity Z . We show models A5F05 (fiducial), HIGH_MASS, SMALL_M2, LOW_SPIN, HIGH_SPIN, SHORT_DELAY, LONG_DELAY, BROAD_VESC, NARROW_VESC.

a small dependence on metallicity. For other models, the percentage of N_g BBHs can be as low as $\sim 8\%$ (HIGH_SPIN case) or as high as $\sim 40\text{--}50\%$ (LOW_SPIN case). For GCs and YSCs these percentages should be lowered by a factor of ~ 30 and $\sim 10^3$, respectively. Table 2 reports the values of $f_{>1g}$ in detail.

3.2. BHs in the mass gap and IMBHs

Hierarchical mergers could be responsible for the formation of BHs with mass in the PI mass gap ($\sim 60\text{--}120 M_\odot$) or even in the IMBH regime ($> 100 M_\odot$). The bottom left panel of Figure 8 shows $f_{\text{PI SN}}$ defined as $f_{\text{PI SN}} = N_{\text{PI SN}}/N_{\text{BBH}}$, where $N_{\text{PI SN}}$ is the number of BBH mergers with primary mass in the PI mass gap, while N_{BBH} is the number of all BBH mergers. In our fiducial model and in NSCs, $\sim 0.7\%$ of all BBH mergers contain at least one BH in the PI mass gap at the lowest metallicity ($Z = 0.0002$). This percentage decreases as metallicity increases and drops to zero at $Z \geq 0.012$. The other models follow the same trend with metallic-

ity. The HIGH_MASS model is the one with the largest value of $f_{\text{PI SN}}$: in this case, up to 7.5% of all the BBH mergers contain at least one BH in the PI mass gap at the lowest metallicity ($Z = 0.0002$). These percentages should be lowered by a factor of $\gtrsim 10$ in GCs and by a factor of $\sim 10^3$ in YSCs.

In the bottom right panel of Figure 8, we show the fraction of IMBH mergers f_{IMBH} , defined as $f_{\text{IMBH}} = N_{\text{IMBH}}/N_{\text{BBH}}$, where N_{IMBH} is the number of BBH mergers with primary mass $m_1 > 10^2 M_\odot$. The fraction of IMBH mergers follows the same trend with metallicity as $f_{\text{PI SN}}$: it is higher at lower Z and drops to zero at $Z \geq 4 \times 10^{-3}$. In the fiducial model, $f_{\text{IMBH}} \sim 5 \times 10^{-4}$ at $Z = 0.0002$ in NSCs. We find no IMBHs in GCs and YSCs in the fiducial case.

The fraction of IMBH mergers is maximum in the SMALL_M2 simulation, where $f_{\text{IMBH}} \sim 2 \times 10^{-2}$ at $Z = 0.0002$. Moreover, $f_{\text{IMBH}} \sim 6 \times 10^{-4}$ and $\sim 3 \times 10^{-5}$ at $Z = 0.0002$ in the HIGH_MASS case for GCs and

Table 2. Values of $f_{>1g}$, f_{PISN} and f_{IMBH} for different runs.

Run Name	Star cluster	$f_{>1g}$	f_{PISN}	f_{IMBH}
Fiducial, A5F05	NSC	0.16, 0.15, 0.13	0.007, 0.009, 0	0.0005, 0.0005, 0
	GC	0.006, 0.007, 0.005	0.0003, 0.0005, 0	0, 0, 0
	YSC	0.0001, 0.0002, 0	5×10^{-6} , 2×10^{-5} , 0	0, 0, 0
A5F01	NSC	0.14, 0.11, 0.13	0.003, 7×10^{-5} , 0	0.0002, 0, 0
	GC	0.005, 0.002, 0	0.0002, 0, 0	0, 0, 0
	YSC	0.0001, 5×10^{-5} , 0	10^{-5} , 0, 0	0, 0, 0
A5F1	NSC	0.14, 0.16, 0.15	0.014, 0.020, 0	0.0008, 0.0008, 0
	GC	0.004, 0.008, 0.004	0.0007, 0.0013, 0	5×10^{-7} , 0, 0
	YSC	9×10^{-5} , 0.0003, 0.004	2×10^{-5} , 4×10^{-5} , 0	0, 0, 0
HIGH_MASS	NSC	0.26, 0.25, 0.15	0.075, 0.055, 0	0.016, 0.011, 0
	GC	0.009, 0.007, 0.005	0.004, 0.003, 0	0.0006, 0.0006, 0
	YSC	9×10^{-5} , 8×10^{-5} , 0	4×10^{-5} , 3×10^{-5} , 0	3×10^{-5} , 3×10^{-5} , 0
SMALL_M2	NSC	0.18, 0.19, 0.14	0.009, 0.014, 0	0.019, 0.038, 0
	GC	0.006, 0.007, 0.003	0.0003, 0.0004, 0	0, 0, 0
	YSC	0.0001, 0.0002, 0.0026	10^{-5} , 10^{-5} , 0	0, 0, 0
LOW_SPIN	NSC	0.45, 0.43, 0.37	0.021, 0.029, 0	0.0009, 0.0011, 0
	GC	0.11, 0.15, 0.11	0.007, 0.012, 0	2×10^{-6} , 4×10^{-6} , 0
	YSC	0.013, 0.020, 0.013	0.0010, 0.0008, 0	0, 0, 0
HIGH_SPIN	NSC	0.08, 0.08, 0.09	0.004, 0.004, 0	0.0002, 0.0003, 0
	GC	0.002, 0.003, 0.003	0.0001, 0.0002, 0	0, 0, 0
	YSC	4×10^{-5} , 4×10^{-5} , 0	9×10^{-7} , 0, 0	0, 0, 0
SHORT_DELAY	NSC	0.16, 0.15, 0.12	0.007, 0.010, 0	0.0005, 0.0006, 0
	GC	0.006, 0.007, 0.005	0.0003, 0.0005, 0	9×10^{-7} , 0, 0
	YSC	0.0001, 0.0002, 0	6×10^{-6} , 9×10^{-6} , 0	0, 0, 0
LONG_DELAY	NSC	0.16, 0.15, 0.14	0.007, 0.010, 0	0.0004, 0.0006, 0
	GC	0.006, 0.007, 0.003	0.0003, 0.0005, 0	0, 0, 0
	YSC	0.0001, 0.0002, 0	7×10^{-6} , 10^{-5} , 0	0, 0, 0
BROAD_VESC	NSC	0.20, 0.20, 0.16	0.012, 0.015, 0	0.004, 0.005, 0
	GC	0.012, 0.013, 0.003	0.0006, 0.0009, 0	4×10^{-6} , 8×10^{-6} , 0
	YSC	0.0004, 0.0005, 0	3×10^{-5} , 3×10^{-5} , 0	0, 0, 0
NARROW_VESC	NSC	0.14, 0.13, 0.08	0.006, 0.007, 0	0.0001, 0.0001, 0
	GC	0.003, 0.005, 0	0.0002, 0.0003, 0	0, 0, 0
	YSC	8×10^{-5} , 0.0001, 0	7×10^{-6} , 4×10^{-6} , 0	0, 0, 0

NOTE—Column 1: Name of the model. Column 2: star cluster type (NSC, GC or YSC). Column 3: fraction of N_g BBHs $f_{>1g}$. The three values reported in each line refer to $Z = 0.0002, 0.002$ and 0.02 . Column 4: fraction of BBHs with primary mass in the PI gap f_{PISN} . The three values reported in each line refer to $Z = 0.0002, 0.002$ and 0.02 . Column 5: fraction of IMBH mergers f_{IMBH} . The three values reported in each line refer to $Z = 0.0002, 0.002$ and 0.02 .

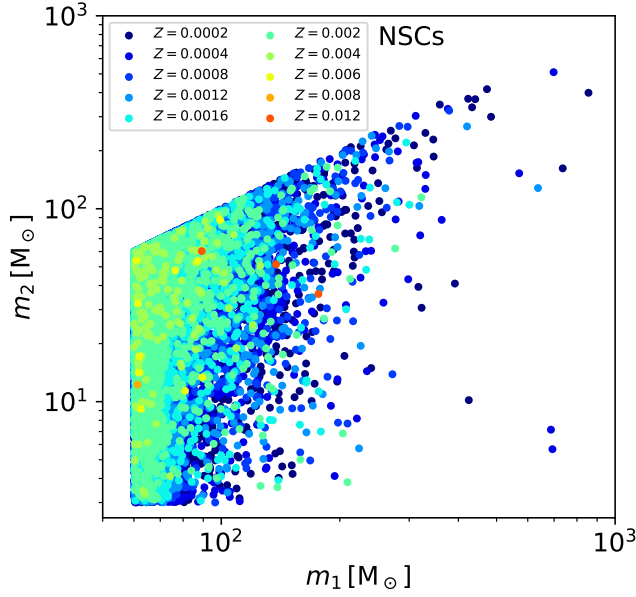


Figure 9. Secondary mass versus primary mass if we consider all Ng BBHs with $m_1 \geq 60 M_\odot$. We show only the fiducial model. The color map shows the metallicity. Metallicities $Z > 0.012$ are not shown because we do not find any BBH with $m_1 \geq 60 M_\odot$ with this metallicity.

YSCs, respectively. Figure 9 shows the masses of BBHs with primary in the PI gap and in the IMBH regime in our fiducial case. The maximum masses strongly depend on progenitor’s metallicity. Table 2 reports the values of f_{PISN} and f_{IMBH} in detail.

3.3. Merger Rates

Figures 10 and 11 show the merger rate density evolution for all our models, calculated as detailed in Section 2.7. The contribution of each channel to the total merger rate density is basically set by the value of $f_i(z)$, because the hierarchical mergers are only a small fraction of the total BBH mergers (see Figure 8). Since $f_i(z)$ is highly uncertain, the relative importance of different channels in Figures 10 and 11 can change wildly and is only indicative. The uncertainty is particularly large for field and YSCs.

Models with $\alpha = 1$ have a higher merger rate than models with $\alpha = 5, 10$. The merger rate evolution of dynamical BBHs in the HIGH_MASS case is remarkably different from the other cases. The reason is our choice of the delay time distribution of 1g BBHs ($dN/dt \propto t^{-1}$), which does not take into account a possible dependence of t_{delay} on the mass and other properties of BBHs. In particular, the delay time distribution obtained with MOBSE tends to deviate from the $dN/dt \propto t^{-1}$ trend when $t_{\text{delay}} < 1$ Gyr. Hence, dy-

namical BBHs in the HIGH_MASS case have shorter delay times than the fiducial case.

Figures 10 and 11 also show the BBH merger rate density we obtain if we consider only Ng BBHs with $N > 1$ in NSCs. In the local Universe, the merger rate density of Ng BBHs in NSCs ranges from $\sim 10^{-2}$ to $\sim 0.2 \text{ Gpc}^{-3} \text{ yr}^{-1}$. For GCs and YSCs we obtain lower values because, even if these star clusters are likely more common than NSCs, the occurrence of Ng BBH mergers in GCs and YSCs is orders of magnitude lower than in NSCs (e.g. Section 3.1).

3.4. Mass Distribution at different redshifts

Figure 12 shows the total mass distribution of primary BHs in the source frame at redshift $z = 1$. NSCs are responsible for the high mass tail ($m_1 \gtrsim 100 M_\odot$) at all redshifts and in all models. We show only the distribution at $z = 1$, because we do not see significant changes of the mass distribution with redshift in all cases but the HIGH_MASS model. In this case, the importance of dynamical BBHs drops at redshift zero because of the different delay time distributions (Figure 11).

Figure 13 shows the mass distribution of primary BHs at redshift $z = 2$ for NSCs only. We separate 1g BBHs from Ng BBHs with $N > 1$. The maximum mass of 1g BBHs extends up to $\sim 40 M_\odot$ in all simulations but the HIGH_MASS case. In the HIGH_MASS case, 1g BHs with mass up to $\sim 100 M_\odot$ are possible, because this model includes BHs that form with mass in the PI gap from the merger of massive stars (Di Carlo et al. 2019c) and acquire companions by dynamical exchanges.

The mass of Ng BHs extends up to $\sim 100 - 200 M_\odot$ in most models, with the exception of the following runs. In the HIGH_MASS case, we find primary BHs with mass up to $\sim 600 - 10^3 M_\odot$. In the SMALL_M2 case, the most massive BH reaches $\sim 5 \times 10^4 M_\odot$. Finally, this realization of the BROAD_VESC model produces one single BH with mass $\sim 4.3 \times 10^5 M_\odot$. To obtain the shown distributions, we started from catalogs of $\geq 10^6$ BBHs. Figure 13 confirms that the distribution of Ng BBHs strongly depends not only on the properties of the environment (e.g. v_{esc}) but also on the mass distribution of 1g BHs.

3.5. Comparison with LVC BBHs in the first and second observing runs

To compare our models against LVC events in the first and second observing runs (O1 and O2, respectively), we use a hierarchical Bayesian approach. In this framework, the posterior for a set of data $\{h\}^k$ observed during an observation time T_{obs} and a model parametrized by λ is well described by an in-homogeneous Poisson process (Loredo 2004; Mandel et al. 2019)

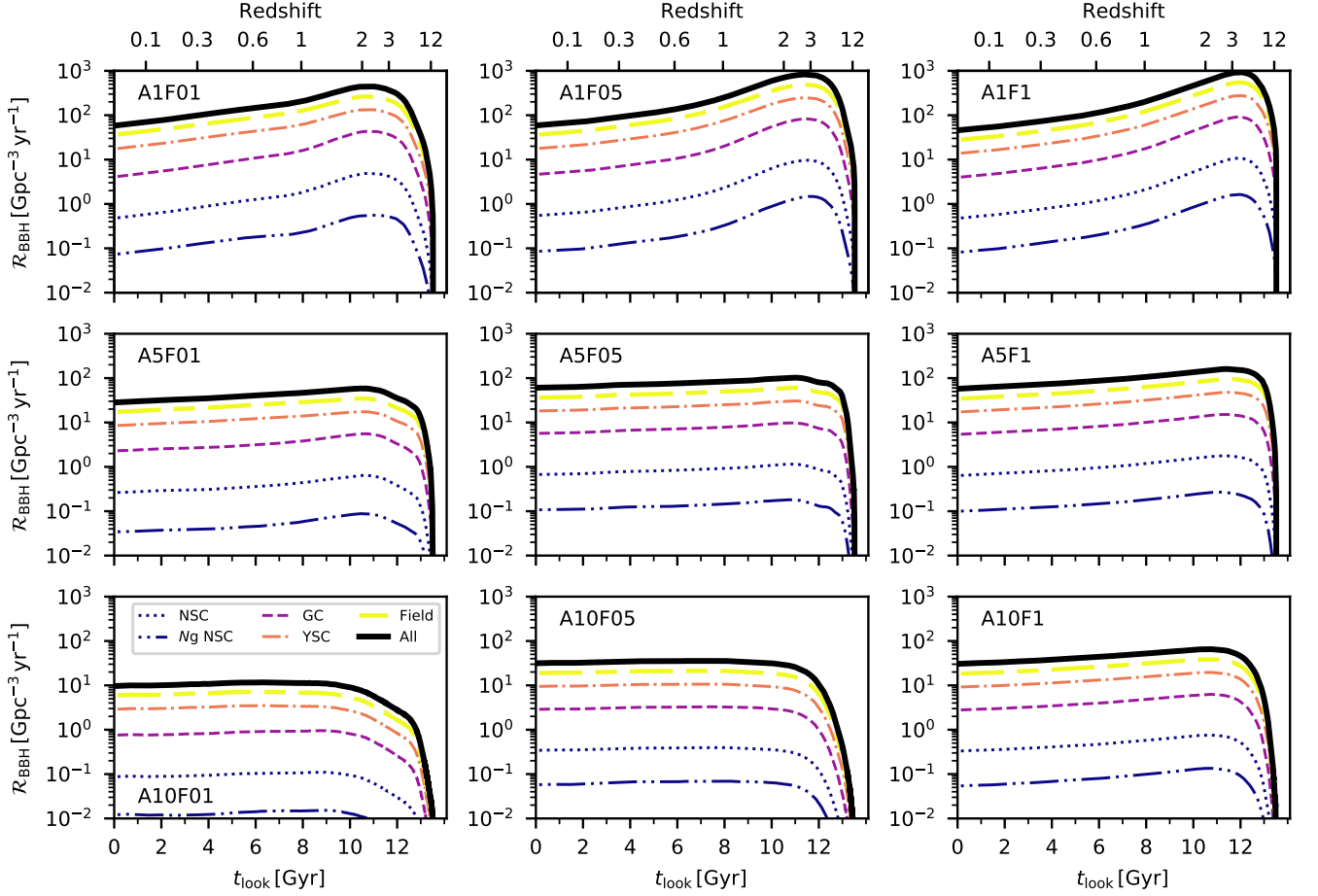


Figure 10. From top to bottom and from left to right: BBH merger rate density in the comoving frame as a function of look-back time (bottom x -axis) and redshift (top x -axis) for the simulations A1F01, A1F05, A1F1, A5F01, A5F05, A5F1, A10F01, A10F05, A10F1. Black thick line: total merger rate density; yellow long-short dashed line: BBH merger rate density from field binaries; pink dot-dashed line: BBH merger rate density from YSCs; violet dashed line: BBH merger rate density from GCs; blue dotted line: BBH merger rate density from NSCs; blue dot-dot-dashed line: BBH merger rate density from NSCs if we consider only N_g BBHs with $N > 1$.

$$p(\lambda|\{h\}^k) \sim e^{-\mu_\lambda} p(\lambda) \prod_{k=1}^{N_{obs}} N_\lambda \int_{\theta} \mathcal{L}^k(d|\theta) p_\lambda(\theta) d\theta, \quad (14)$$

where N_λ is the number of sources predicted by the model, μ_λ is the predicted number of detections during T_{obs} , θ are the GW parameters, $\mathcal{L}^k(d|\theta)$ is the likelihood of the k th detection and $p_\lambda(\theta)$ is the distribution of the model as a function of θ . In practice, for each model, we generate a catalog of a fixed number of sources (fixed to 50000 sources), such that the sources are distributed according to the merger rate density of the model. Each entry of the catalog is represented by a set of parameters $\theta = \mathcal{M}_c, q, z$ where \mathcal{M}_c is the chirp mass of the source, q the mass ratio, and z the redshift that was set to take values between 0 and 2. Using kernel den-

sity estimation, we can then use this catalog of sources to compute the model distribution $p_\lambda(\theta)$ at each value θ . Finally, the number of sources N_λ is computed using the merger rate density estimation, while the expected number of detections is evaluated following the usual approach involving the computation of VT. More details on this procedure are described in Mandel et al. (2019) and Bouffanais et al. (2019).

From the model posterior in eq. 14, we can directly compute the odds ratio between model 1 and 2 as

$$\mathcal{O}_{\lambda_1|\lambda_2} = \frac{p(\lambda_1|\{h\}^k)}{p(\lambda_2|\{h\}^k)} \quad (15)$$

Note that the proportionality sign is replaced by an equality in the odds ratio, as both models have the same proportionality constant that cancels out when dividing the two terms. Also, we have considered an uniform prior over all possible models, so that the prior term

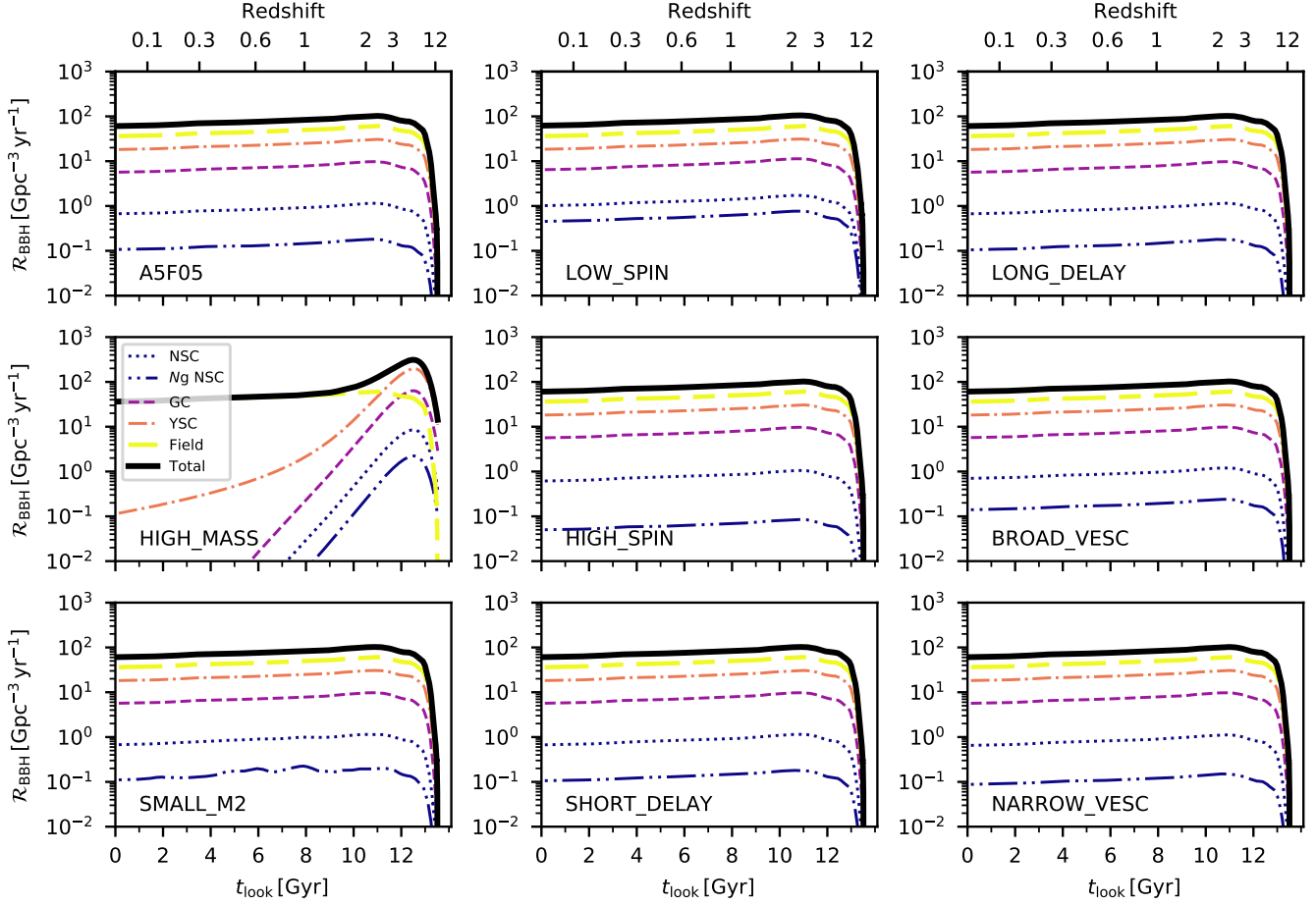


Figure 11. Same as Figure 10 but for the simulations A5F05, HIGH_MASS, SMALL_M2, LOW_SPIN, HIGH_SPIN, SHORT_DELAY, LONG_DELAY, BROAD_VESC, NARROW_VESC.

Table 3. Odds ratios with respect to the fiducial model (A5F05).

Run Name	Odds ratios
A5F05	1.0
HIGH_MASS	4.4×10^{-7}
SMALL_M2	8.3×10^{-1}
LOW_SPIN	5.1×10^3
HIGH_SPIN	1.3×10^{-5}
SHORT_DELAY	5.7
LONG_DELAY	1.9×10^{-2}
BROAD_VESC	1.3×10^2
NARROW_VESC	2.3×10^{-1}

NOTE—Column 1: Name of the model. Column 2: value of the odds ratio between the model in the first column and our reference model A5F05.

also cancels out. Table 3 shows the odds ratio of the models with respect to our reference model A5F05. Our results suggest that amongst our list of models, the models LOW_SPIN, BROAD_VESC and SHORT_DELAY are favored by current LVC data, while the models HIGH_SPIN and HIGH_MASS seem to be already rejected. These results need to be nuanced by the fact that the analysis is done with only a small number of events (10 BBHs) to constrain a complicated distribution in four-dimensions.

4. DISCUSSION OF THE MAIN CAVEATS

We presented a new model that can be used to rapidly simulate hierarchical mergers in different environments (NSCs, GCs and YSCs), exploring a broad parameter space (e.g. progenitor’s metallicity, binary evolution parameters such as α and f_{MT} , escape velocity from the parent star cluster, delay times and 1g spin distribution).

The treatment of dynamical pairing of N_g BBHs is still approximate: we assume that the retained merger

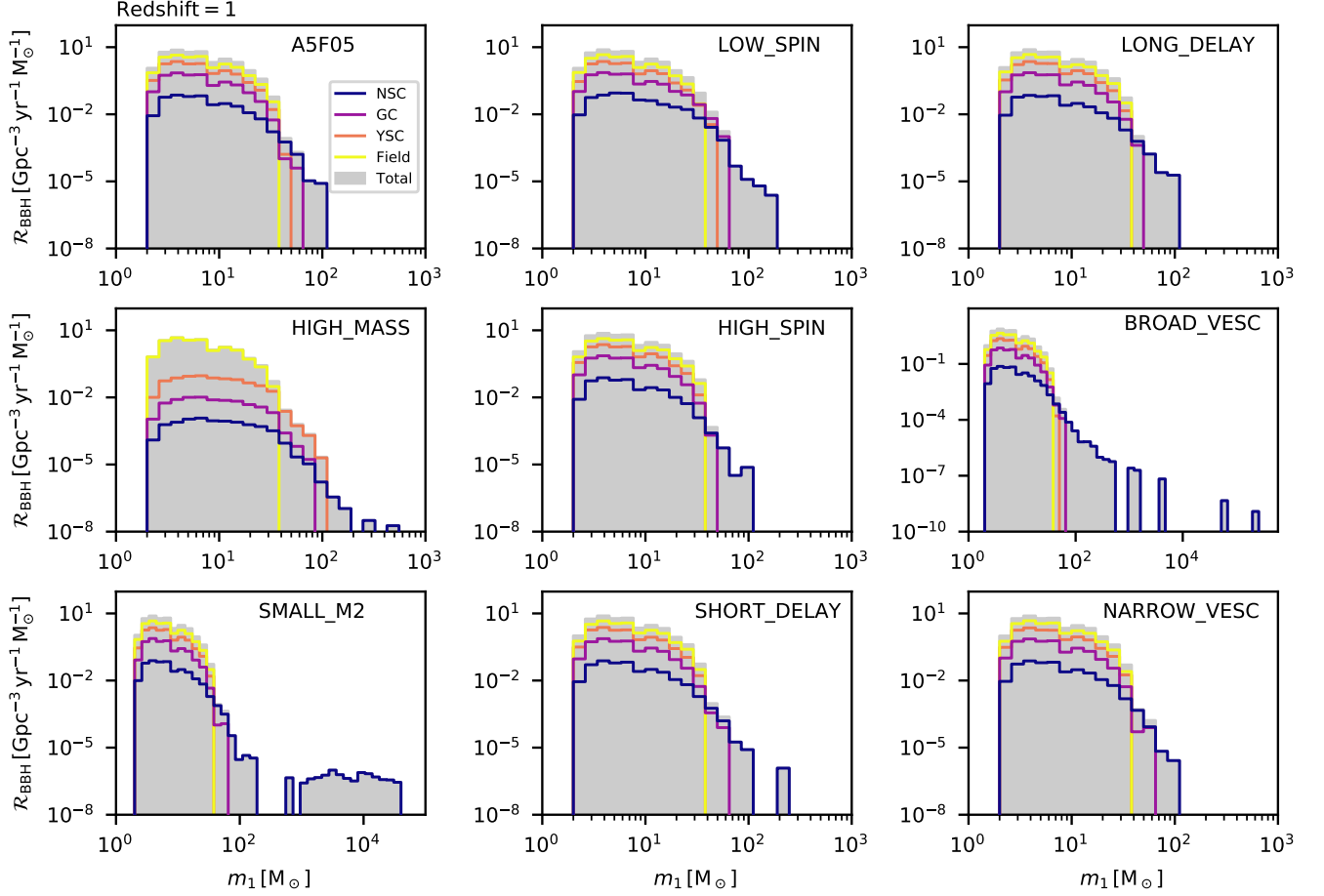


Figure 12. From top to bottom and from left to right: merger rate density per unit primary mass as a function of BBH mass at redshift $z = 1$ for the simulations A5F05, HIGH_MASS, SMALL_M2, LOW_SPIN, HIGH_SPIN, SHORT_DELAY, LONG_DELAY, BROAD_VESC, NARROW_VESC. Grey histogram: sum of all formation channels; yellow: field binaries; pink: YSCs; violet: GCs; blue: NSCs.

remnants find a new companion and merge over a timescale $dN/dt \propto t^{-1}$. This is in agreement with the findings of Antonini et al. (2019), but could be improved with an analytic treatment of dynamical hardening. Furthermore, we assume that BHs are ejected only by relativistic kicks, i.e. we neglect dynamical recoil via close encounters. Finally, we assume that the star cluster does not evolve with time: it has a constant escape velocity. As shown in previous work (Breen & Heggie 2013a,b; Morscher et al. 2015; Wang 2020), the properties of the star cluster might change significantly with time and the growth of an IMBH is strongly linked to the evolution of the host star cluster. For example, if we assume constant cluster mass, the half-mass ratio is expected to grow as $r_h \propto t^{2/3}$ and the escape velocity to decrease with time as $v_{\text{esc}} \propto t^{-1/3}$ (Hénon 1965). These two effects might slow down or even suppress the growth of an IMBH in the late evolutionary stages (e.g. Antonini et al. 2019).

In our fiducial model, we assume that the stellar binaries which give birth to first-generation BHs are primordial binaries and are not ionized by dynamical interactions. This assumption is motivated by the properties of such binaries. A BBH merger progenitor has an initial binding energy

$$E_b \sim 6 \times 10^{49} \text{ erg s}^{-1} \left(\frac{m_1}{50 M_\odot} \right) \left(\frac{m_2}{50 M_\odot} \right) \left(\frac{1000 R_\odot}{a} \right), \quad (16)$$

where a is the initial semi-major axis. The typical kinetic energy of a star in a star cluster is

$$E_K \sim 10^{47} \text{ erg s}^{-1} \left(\frac{\langle m \rangle}{1 M_\odot} \right) \left(\frac{\sigma_{\text{SC}}}{100 \text{ km s}^{-1}} \right)^2, \quad (17)$$

where $\langle m \rangle$ is the average stellar mass in the cluster and σ_{SC} is the velocity dispersion. In the example, we consider an extremely high velocity dispersion $\sigma_{\text{SC}} = 100 \text{ km s}^{-1}$. Hence, binaries that will produce BBH mergers are hard binaries even in the most extreme star clusters

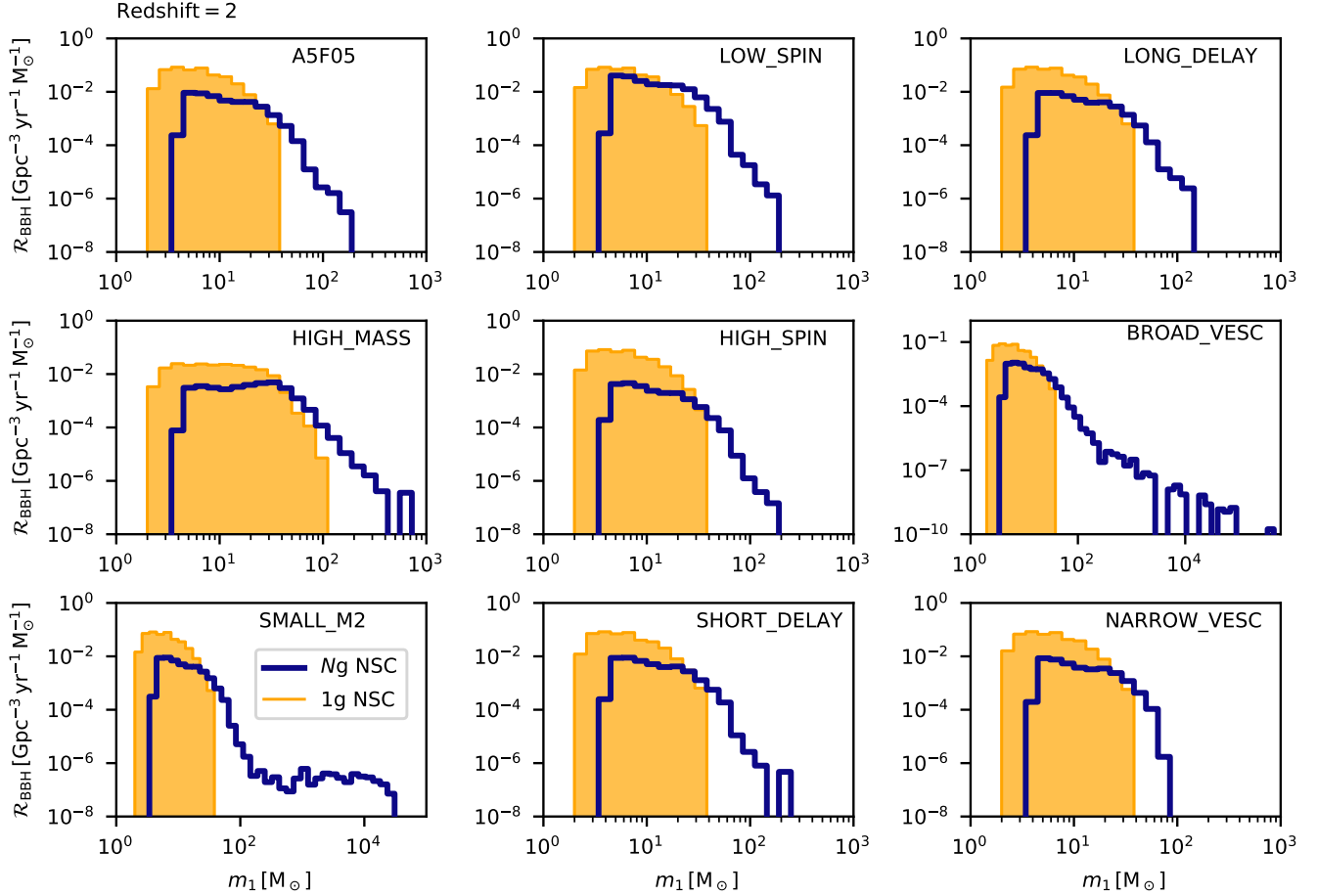


Figure 13. Merger rate density per unit primary mass as a function of BBH mass at redshift $z = 2$ for BBHs in NSCs. Filled orange histogram: 1g BBHs; blue histogram: N_g BBHs with $N > 1$. From top to bottom and from left to right: simulations A5F05, HIGH_MASS, SMALL_M2, LOW_SPIN, HIGH_SPIN, SHORT_DELAY, LONG_DELAY, BROAD_VESC, NARROW_VESC.

and survive ionization. This assumption breaks in the immediate vicinity of a super-massive BH. For example, inside the influence radius of a supermassive BH with mass $m_{\text{BH}} = 10^6 M_\odot$, the typical velocities are $\sim 120 \text{ km s}^{-1} (a/0.01 \text{ pc})^{-1/2} (m_{\text{BH}}/10^6 M_\odot)$. In this extreme case, even BBHs and their stellar progenitors might be soft binaries and might be broken. On the other hand, dynamical hardening might also be very effective as the BBH gets closer to a supermassive BH by dynamical friction, allowing the BBH to avoid ionization and even speeding up its merger (Arca Sedda 2020).

Here, we make no assumptions about the formation of NSCs. If some of them, if not all, are formed by the hierarchical assembly of GCs (Tremaine et al. 1975; Capuzzo-Dolcetta 1993), this might have a crucial impact on the population of BBHs. In fact, the GCs might be already depleted of merger remnants (because of the relatively low escape velocity) before merging to build up the NSC.

Moreover, we neglect the AGN disk formation channel (McKernan et al. 2012; Stone et al. 2017; Bartos et al. 2017; McKernan et al. 2018; Yang et al. 2020). Including the physics of AGN disks can boost the contribution of galactic nuclei to the total merger rate and to N_g mergers. AGN disk physics can further speed up the pairing and merger of our BHs. We will include the AGN disk scenario in future work.

In Arca Sedda et al. (2020), we found remnant masses only up to $\sim 200 M_\odot$, significantly lower than the results presented here for most models. The main reason for this difference is that Arca Sedda et al. (2020) fixed the escape velocity from NSCs to $v_{\text{esc}} = 100 \text{ km s}^{-1}$ and did not change this parameter. Our results are consistent with other models (e.g. Antonini et al. 2019), where higher values of v_{esc} are explored. This result is remarkable when considering that Antonini et al. (2019) adopt a more accurate model for dynamical interactions than the one presented here. Hence, escape velocities

are the key ingredient to understand the mass spectrum of BHs in NSCs.

Finally, we include a simple redshift dependence based on the $f_i(t)$ functions. Alternative redshift dependencies can be obtained by changing $f_i(t)$. For example, if we assume $f_{\text{NSC}} = 0.1$ (constant with redshift), we obtain an upper limit to the merger rate density associated with NSCs, because they are unlikely to contribute to 10% of the overall cosmic star formation rate. Under such extreme assumption, the local BBH merger rate density from NSCs is $\mathcal{R}_{\text{NSC}} \approx 7 - 10 \text{ Gpc}^{-3} \text{ yr}^{-1}$, i.e. approximately a factor of 10 higher than the models we presented in Figures 10 and 11.

5. CONCLUSIONS

Hierarchical mergers in dynamical environments can lead to the formation of BHs with mass higher than the limits imposed by PI, core-collapse SNe and stellar evolution theory. Here, we have presented a fast Monte Carlo method to draw the main properties (masses, spins, merger rate) of hierarchical BBHs, while probing the relevant parameter space.

In our models, NSCs are the dominant environment for the formation of hierarchical BBHs. In our fiducial model (A5F05), primary BHs with mass up to $\sim 10^3 M_\odot$ can form in NSCs, while the maximum primary BH mass is $\sim 100 M_\odot$ for both GCs and YSCs.

We find that the mass distribution of first-generation (1g) BBHs has a crucial impact on the mass distribution of N_g BHs with $N > 1$. The metallicity of the progenitor is a key ingredient to shape the distribution of N_g BBHs, because it affects both the number and the maximum mass of BBHs. The common envelope α parameter and the accretion efficiency f_{MT} also play a role, with smaller values of α leading to higher merger rates and higher values of f_{MT} leading to more top-heavy BH mass functions.

If BHs with mass in the PI gap are allowed to form by stellar mergers (Di Carlo et al. 2019c), the mass distribution of N_g BBHs is skewed toward significantly larger masses (HIGH_MASS model). Primary BH masses up to a few $\times 10^4 M_\odot$ can be obtained in NSCs if only N_g -1g mergers are allowed to take place, i.e. if we prevent the secondary BH from being a merger remnant itself (SMALL_M2 model). The main reason is that relativistic kicks are smaller if the mass ration $q = m_2/m_1$ tends to zero.

The escape velocity from the parent star cluster (v_{esc}) is probably the most important parameter to set the maximum BH mass. If we assume that the distribution of escape velocities from NSCs is $\log_{10}(v_{\text{esc}}/\text{km s}^{-1}) = 2 \pm 0.3$ (BROAD_VESC model), BHs with mass up to

$\sim 10^6 M_\odot$ are allowed to form in the NSCs with the highest escape velocities. This result is consistent with Antonini et al. (2019) and Fragione & Silk (2020).

While BBHs in GCs and YSCs do not exceed the 5th and the 3rd generation, respectively, we expect at least 10 different BBH generations in NSCs. This number grows up to few thousands if N_g -1g BBHs are the only way to produce hierarchical mergers (SMALL_M2 model).

In our fiducial model, the fraction of N_g BBHs is $f_{>1g} \sim 0.15$ in NSCs, which lowers to 6×10^{-3} in GCs and $\sim 10^{-4}$ in YSCs. In the most optimistic case (i.e. when low spins are assumed for 1g BHs), $f_{>1g} \sim 0.5, 0.1, 0.01$ for NSCs, GCs and YSCs, respectively. In the most pessimistic case (i.e. when high spins are assumed), $f_{>1g} \sim 0.08, 2 \times 10^{-3}$ and 4×10^{-5} for NSCs, GCs and YSCs, respectively.

BHs in the PI mass gap and IMBHs can form via hierarchical mergers. Their fraction is strongly suppressed at high metallicity. At $Z = 0.0002$ and in our fiducial model, the fraction of BBH mergers with primary BH mass in the PI gap is $f_{\text{PISN}} \sim 7 \times 10^{-3}, 3 \times 10^{-4}$ and 5×10^{-6} in NSCs, GCs and YSCs, respectively. In our fiducial model, the fraction of BBH mergers with primary BH mass in the IMBH regime is $f_{\text{IMBH}} \sim 5 \times 10^{-4}$ in NSCs, while we do not find any IMBH mergers in either GCs or YSCs. These fractions are significantly higher in the SMALL_M2 and in the HIGH_MASS models (Figure 8).

The local BBH merger rates in our models range from ~ 10 to $\sim 60 \text{ Gpc}^{-3} \text{ yr}^{-1}$, but N_g BBHs in NSCs account for only $10^{-2} - 0.2 \text{ Gpc}^{-3} \text{ yr}^{-1}$ in our models. If we assume that 10% of all stars form in NSCs, we find a robust upper limit $\sim 7 - 10 \text{ Gpc}^{-3} \text{ yr}^{-1}$ for the local merger rate density of N_g BBHs in NSCs.

We compare our models against LIGO–Virgo data from the first and second observing runs. Models with low spins (LOW_SPIN) and a broad distribution of escape velocities (BROAD_VESC) seem to be favored by these LVC data. It will be crucial to compare the results of our models with data from the third observing run.

ACKNOWLEDGMENTS

We thank Eugenio Carretta for useful discussion and we thank the internal referee of the LVC, Fabio Antonini, for his suggestions, which helped us improve this work. MM, FS, YB, NG and AB acknowledge financial support from the European Research Council for the ERC Consolidator grant DEMOBLACK, under contract no. 770017. MM and MCA acknowledges financial support from the Austrian National Science Foundation through FWF stand-alone grant P31154-N27. MAS acknowledges financial support from the Alexander von Humboldt Foundation for the research program “The evolution of black holes from stellar to galactic scales”, the Volkswagen Foundation Trilateral Partnership for project No. I/97778 “Dynamical Mechanisms of Accretion in Galactic Nuclei”, and the Deutsche Forschungsgemeinschaft (DFG, German Research Foundation) – Project-ID 138713538 – SFB 881 “The Milky Way System”.

Software: HIERBLACK (this paper), COSMORATE (Santoliquido et al. 2020), MOBSE (Giacobbo et al. 2018)

REFERENCES

- Aasi, J., Abbott, B. P., Abbott, R., et al. 2015, *Classical and Quantum Gravity*, 32, 074001.
<http://stacks.iop.org/0264-9381/32/i=7/a=074001>
- Abbott, B. P., Abbott, R., Abbott, T. D., et al. 2016, *Phys. Rev. Lett.*, 116, 061102,
doi: [10.1103/PhysRevLett.116.061102](https://doi.org/10.1103/PhysRevLett.116.061102)
- Abbott, B. P., Abbott, R., Abbott, T. D., et al. 2016a, *ApJL*, 818, L22, doi: [10.3847/2041-8205/818/2/L22](https://doi.org/10.3847/2041-8205/818/2/L22)
- . 2016b, *Physical Review X*, 6, 041015,
doi: [10.1103/PhysRevX.6.041015](https://doi.org/10.1103/PhysRevX.6.041015)
- . 2017, *Physical Review Letters*, 119, 161101,
doi: [10.1103/PhysRevLett.119.161101](https://doi.org/10.1103/PhysRevLett.119.161101)
- . 2019a, *Physical Review X*, 9, 031040,
doi: [10.1103/PhysRevX.9.031040](https://doi.org/10.1103/PhysRevX.9.031040)
- . 2019b, *ApJL*, 882, L24, doi: [10.3847/2041-8213/ab3800](https://doi.org/10.3847/2041-8213/ab3800)
- . 2020a, *ApJL*, 892, L3, doi: [10.3847/2041-8213/ab75f5](https://doi.org/10.3847/2041-8213/ab75f5)
- Abbott, R., Abbott, T. D., Abraham, S., et al. 2020b, *arXiv e-prints*, arXiv:2004.08342.
<https://arxiv.org/abs/2004.08342>
- . 2020c, *ApJL*, 896, L44, doi: [10.3847/2041-8213/ab960f](https://doi.org/10.3847/2041-8213/ab960f)
- Acernese, F., Agathos, M., Agatsuma, K., et al. 2015, *Classical and Quantum Gravity*, 32, 024001,
doi: [10.1088/0264-9381/32/2/024001](https://doi.org/10.1088/0264-9381/32/2/024001)
- Ade, P. A. R., Aghanim, N., & Zonca, A. e. a. 2016, *A&A*, 594, A13, doi: [10.1051/0004-6361/201525830](https://doi.org/10.1051/0004-6361/201525830)
- Antonini, F. 2013, *ApJ*, 763, 62,
doi: [10.1088/0004-637X/763/1/62](https://doi.org/10.1088/0004-637X/763/1/62)
- Antonini, F., Capuzzo-Dolcetta, R., Mastrobuono-Battisti, A., & Merritt, D. 2012, *ApJ*, 750, 111,
doi: [10.1088/0004-637X/750/2/111](https://doi.org/10.1088/0004-637X/750/2/111)
- Antonini, F., Chatterjee, S., Rodriguez, C. L., et al. 2016, *ApJ*, 816, 65, doi: [10.3847/0004-637X/816/2/65](https://doi.org/10.3847/0004-637X/816/2/65)
- Antonini, F., & Gieles, M. 2020, *MNRAS*, 492, 2936,
doi: [10.1093/mnras/stz3584](https://doi.org/10.1093/mnras/stz3584)
- Antonini, F., Gieles, M., & Gualandris, A. 2019, *MNRAS*, 486, 5008, doi: [10.1093/mnras/stz1149](https://doi.org/10.1093/mnras/stz1149)
- Antonini, F., & Rasio, F. A. 2016, *ApJ*, 831, 187,
doi: [10.3847/0004-637X/831/2/187](https://doi.org/10.3847/0004-637X/831/2/187)
- Antonini, F., Toonen, S., & Hamers, A. S. 2017, *ApJ*, 841, 77, doi: [10.3847/1538-4357/aa6f5e](https://doi.org/10.3847/1538-4357/aa6f5e)
- Arca Sedda, M. 2020, *ApJ*, 891, 47,
doi: [10.3847/1538-4357/ab723b](https://doi.org/10.3847/1538-4357/ab723b)
- Arca Sedda, M., & Benacquista, M. 2019, *MNRAS*, 482, 2991, doi: [10.1093/mnras/sty2764](https://doi.org/10.1093/mnras/sty2764)
- Arca-Sedda, M., & Capuzzo-Dolcetta, R. 2014, *MNRAS*, 444, 3738, doi: [10.1093/mnras/stu1683](https://doi.org/10.1093/mnras/stu1683)
- . 2019, *MNRAS*, 483, 152, doi: [10.1093/mnras/sty3096](https://doi.org/10.1093/mnras/sty3096)

- Arca-Sedda, M., Capuzzo-Dolcetta, R., Antonini, F., & Seth, A. 2015, *ApJ*, 806, 220, doi: [10.1088/0004-637X/806/2/220](https://doi.org/10.1088/0004-637X/806/2/220)
- Arca-Sedda, M., & Gualandris, A. 2018, *MNRAS*, 477, 4423, doi: [10.1093/mnras/sty922](https://doi.org/10.1093/mnras/sty922)
- Arca-Sedda, M., Li, G., & Kocsis, B. 2018, arXiv e-prints, arXiv:1805.06458. <https://arxiv.org/abs/1805.06458>
- Arca Sedda, M., Mapelli, M., Spera, M., Benacquista, M., & Giacobbo, N. 2020, *ApJ*, 894, 133, doi: [10.3847/1538-4357/ab88b2](https://doi.org/10.3847/1538-4357/ab88b2)
- Askar, A., Szkudlarek, M., Gondek-Rosińska, D., Giersz, M., & Bulik, T. 2017, *MNRAS*, 464, L36, doi: [10.1093/mnras/rlw177](https://doi.org/10.1093/mnras/rlw177)
- Banerjee, S. 2017, *MNRAS*, 467, 524, doi: [10.1093/mnras/stw3392](https://doi.org/10.1093/mnras/stw3392)
- . 2018, *MNRAS*, 473, 909, doi: [10.1093/mnras/stx2347](https://doi.org/10.1093/mnras/stx2347)
- . 2020, arXiv e-prints, arXiv:2004.07382. <https://arxiv.org/abs/2004.07382>
- Banerjee, S., Baumgardt, H., & Kroupa, P. 2010, *MNRAS*, 402, 371, doi: [10.1111/j.1365-2966.2009.15880.x](https://doi.org/10.1111/j.1365-2966.2009.15880.x)
- Bartos, I., Kocsis, B., Haiman, Z., & Márka, S. 2017, *ApJ*, 835, 165, doi: [10.3847/1538-4357/835/2/165](https://doi.org/10.3847/1538-4357/835/2/165)
- Belczynski, K., Holz, D. E., Bulik, T., & O’Shaughnessy, R. 2016a, *Nature*, 534, 512, doi: [10.1038/nature18322](https://doi.org/10.1038/nature18322)
- Belczynski, K., Kalogera, V., & Bulik, T. 2002, *ApJ*, 572, 407, doi: [10.1086/340304](https://doi.org/10.1086/340304)
- Belczynski, K., Kalogera, V., Rasio, F. A., et al. 2008, *ApJS*, 174, 223, doi: [10.1086/521026](https://doi.org/10.1086/521026)
- Belczynski, K., Heger, A., Gladysz, W., et al. 2016b, *A&A*, 594, A97, doi: [10.1051/0004-6361/201628980](https://doi.org/10.1051/0004-6361/201628980)
- Belczynski, K., Klencki, J., Fields, C. E., et al. 2020, *A&A*, 636, A104, doi: [10.1051/0004-6361/201936528](https://doi.org/10.1051/0004-6361/201936528)
- Bethe, H. A., & Brown, G. E. 1998, *ApJ*, 506, 780, doi: [10.1086/306265](https://doi.org/10.1086/306265)
- Bird, S., Cholis, I., Muñoz, J. B., et al. 2016, *Physical Review Letters*, 116, 201301, doi: [10.1103/PhysRevLett.116.201301](https://doi.org/10.1103/PhysRevLett.116.201301)
- Bouffanais, Y., Mapelli, M., Gerosa, D., et al. 2019, arXiv e-prints, arXiv:1905.11054. <https://arxiv.org/abs/1905.11054>
- Breen, P. G., & Hogg, D. C. 2013a, *MNRAS*, 432, 2779, doi: [10.1093/mnras/stt628](https://doi.org/10.1093/mnras/stt628)
- . 2013b, *MNRAS*, 436, 584, doi: [10.1093/mnras/stt1599](https://doi.org/10.1093/mnras/stt1599)
- Campanelli, M., Lousto, C., Zlochower, Y., & Merritt, D. 2007, *ApJL*, 659, L5, doi: [10.1086/516712](https://doi.org/10.1086/516712)
- Capuzzo-Dolcetta, R. 1993, *ApJ*, 415, 616, doi: [10.1086/173189](https://doi.org/10.1086/173189)
- Capuzzo-Dolcetta, R., & Miocchi, P. 2008, *MNRAS*, 388, L69, doi: [10.1111/j.1745-3933.2008.00501.x](https://doi.org/10.1111/j.1745-3933.2008.00501.x)
- Carr, B., Kühnel, F., & Sandstad, M. 2016, *PhRvD*, 94, 083504, doi: [10.1103/PhysRevD.94.083504](https://doi.org/10.1103/PhysRevD.94.083504)
- Carr, B. J., & Hawking, S. W. 1974, *MNRAS*, 168, 399, doi: [10.1093/mnras/168.2.399](https://doi.org/10.1093/mnras/168.2.399)
- de Mink, S. E., & Mandel, I. 2016, *MNRAS*, 460, 3545, doi: [10.1093/mnras/stw1219](https://doi.org/10.1093/mnras/stw1219)
- Di Carlo, U. N., Giacobbo, N., Mapelli, M., et al. 2019a, *MNRAS*, 487, 2947, doi: [10.1093/mnras/stz1453](https://doi.org/10.1093/mnras/stz1453)
- Di Carlo, U. N., Mapelli, M., Bouffanais, Y., et al. 2019b, arXiv e-prints, arXiv:1911.01434. <https://arxiv.org/abs/1911.01434>
- . 2019c, arXiv e-prints, arXiv:1911.01434. <https://arxiv.org/abs/1911.01434>
- Doctor, Z., Wysocki, D., O’Shaughnessy, R., Holz, D. E., & Farr, B. 2020, *ApJ*, 893, 35, doi: [10.3847/1538-4357/ab7fac](https://doi.org/10.3847/1538-4357/ab7fac)
- Dominik, M., Belczynski, K., Fryer, C., et al. 2012, *ApJ*, 759, 52, doi: [10.1088/0004-637X/759/1/52](https://doi.org/10.1088/0004-637X/759/1/52)
- . 2013, *ApJ*, 779, 72, doi: [10.1088/0004-637X/779/1/72](https://doi.org/10.1088/0004-637X/779/1/72)
- Downing, J. M. B., Benacquista, M. J., Giersz, M., & Spurzem, R. 2010, *MNRAS*, 407, 1946, doi: [10.1111/j.1365-2966.2010.17040.x](https://doi.org/10.1111/j.1365-2966.2010.17040.x)
- du Buisson, L., Marchant, P., Podsiadlowski, P., et al. 2020, arXiv e-prints, arXiv:2002.11630. <https://arxiv.org/abs/2002.11630>
- Eldridge, J. J., & Stanway, E. R. 2016, *MNRAS*, 462, 3302, doi: [10.1093/mnras/stw1772](https://doi.org/10.1093/mnras/stw1772)
- Eldridge, J. J., Stanway, E. R., & Tang, P. N. 2019, *MNRAS*, 482, 870, doi: [10.1093/mnras/sty2714](https://doi.org/10.1093/mnras/sty2714)
- Farmer, R., Renzo, M., de Mink, S. E., Marchant, P., & Justham, S. 2019, *ApJ*, 887, 53, doi: [10.3847/1538-4357/ab518b](https://doi.org/10.3847/1538-4357/ab518b)
- Favata, M., Hughes, S. A., & Holz, D. E. 2004, *ApJL*, 607, L5, doi: [10.1086/421552](https://doi.org/10.1086/421552)
- Ferrarese, L., & Merritt, D. 2000, *ApJL*, 539, L9, doi: [10.1086/312838](https://doi.org/10.1086/312838)
- Fishbach, M., Holz, D. E., & Farr, B. 2017, *ApJL*, 840, L24, doi: [10.3847/2041-8213/aa7045](https://doi.org/10.3847/2041-8213/aa7045)
- Fitchett, M. J. 1983, *MNRAS*, 203, 1049, doi: [10.1093/mnras/203.4.1049](https://doi.org/10.1093/mnras/203.4.1049)
- Fragione, G., Ginsburg, I., & Kocsis, B. 2018, *ApJ*, 856, 92, doi: [10.3847/1538-4357/aab368](https://doi.org/10.3847/1538-4357/aab368)
- Fragione, G., & Kocsis, B. 2018, *PhRvL*, 121, 161103, doi: [10.1103/PhysRevLett.121.161103](https://doi.org/10.1103/PhysRevLett.121.161103)
- Fragione, G., & Loeb, A. 2019, *MNRAS*, 486, 4443, doi: [10.1093/mnras/stz1131](https://doi.org/10.1093/mnras/stz1131)
- Fragione, G., & Silk, J. 2020, arXiv e-prints, arXiv:2006.01867. <https://arxiv.org/abs/2006.01867>
- Fragos, T., Andrews, J. J., Ramirez-Ruiz, E., et al. 2019, *ApJL*, 883, L45, doi: [10.3847/2041-8213/ab40d1](https://doi.org/10.3847/2041-8213/ab40d1)

- Fryer, C. L., Belczynski, K., Wiktorowicz, G., et al. 2012, *ApJ*, 749, 91, doi: [10.1088/0004-637X/749/1/91](https://doi.org/10.1088/0004-637X/749/1/91)
- Fuller, J., & Ma, L. 2019, *ApJL*, 881, L1, doi: [10.3847/2041-8213/ab339b](https://doi.org/10.3847/2041-8213/ab339b)
- Gebhardt, K., Bender, R., Bower, G., et al. 2000, *ApJL*, 539, L13, doi: [10.1086/312840](https://doi.org/10.1086/312840)
- Gerosa, D., & Berti, E. 2017, *PhRvD*, 95, 124046, doi: [10.1103/PhysRevD.95.124046](https://doi.org/10.1103/PhysRevD.95.124046)
- . 2019, arXiv e-prints, arXiv:1906.05295, <https://arxiv.org/abs/1906.05295>
- Giacobbo, N., & Mapelli, M. 2018, *MNRAS*, 480, 2011, doi: [10.1093/mnras/sty1999](https://doi.org/10.1093/mnras/sty1999)
- . 2019, *MNRAS*, 482, 2234, doi: [10.1093/mnras/sty2848](https://doi.org/10.1093/mnras/sty2848)
- . 2020, *ApJ*, 891, 141, doi: [10.3847/1538-4357/ab7335](https://doi.org/10.3847/1538-4357/ab7335)
- Giacobbo, N., Mapelli, M., & Spera, M. 2018, *MNRAS*, 474, 2959, doi: [10.1093/mnras/stx2933](https://doi.org/10.1093/mnras/stx2933)
- Gratton, R. G., Bragaglia, A., Carretta, E., et al. 2003, *A&A*, 408, 529, doi: [10.1051/0004-6361:20031003](https://doi.org/10.1051/0004-6361:20031003)
- Gratton, R. G., Fusi Pecci, F., Carretta, E., et al. 1997, *ApJ*, 491, 749, doi: [10.1086/304987](https://doi.org/10.1086/304987)
- Harris, W. E., Harris, G. L. H., & Alessi, M. 2013, *ApJ*, 772, 82, doi: [10.1088/0004-637X/772/2/82](https://doi.org/10.1088/0004-637X/772/2/82)
- Hénon, M. 1965, *Annales d'Astrophysique*, 28, 62
- Hills, J. G., & Fullerton, L. W. 1980, *AJ*, 85, 1281, doi: [10.1086/112798](https://doi.org/10.1086/112798)
- Hofmann, F., Barausse, E., & Rezzolla, L. 2016, *ApJL*, 825, L19, doi: [10.3847/2041-8205/825/2/L19](https://doi.org/10.3847/2041-8205/825/2/L19)
- Holley-Bockelmann, K., Gültekin, K., Shoemaker, D., & Yunes, N. 2008, *ApJ*, 686, 829, doi: [10.1086/591218](https://doi.org/10.1086/591218)
- Hurley, J. R., Tout, C. A., & Pols, O. R. 2002, *MNRAS*, 329, 897, doi: [10.1046/j.1365-8711.2002.05038.x](https://doi.org/10.1046/j.1365-8711.2002.05038.x)
- Ivanova, N., Justham, S., Chen, X., et al. 2013, *A&A Rv*, 21, 59, doi: [10.1007/s00159-013-0059-2](https://doi.org/10.1007/s00159-013-0059-2)
- Jiménez-Forteza, X., Keitel, D., Husa, S., et al. 2017, *PhRvD*, 95, 064024, doi: [10.1103/PhysRevD.95.064024](https://doi.org/10.1103/PhysRevD.95.064024)
- Kimball, C., Talbot, C., Berry, C. P. L., et al. 2020, arXiv e-prints, arXiv:2005.00023, <https://arxiv.org/abs/2005.00023>
- Klencki, J., Moe, M., Gladysz, W., et al. 2018, *A&A*, 619, A77, doi: [10.1051/0004-6361/201833025](https://doi.org/10.1051/0004-6361/201833025)
- Kroupa, P. 2001, *MNRAS*, 322, 231, doi: [10.1046/j.1365-8711.2001.04022.x](https://doi.org/10.1046/j.1365-8711.2001.04022.x)
- Kruckow, M. U., Tauris, T. M., Langer, N., Kramer, M., & Izzard, R. G. 2018, *MNRAS*, 481, 1908, doi: [10.1093/mnras/sty2190](https://doi.org/10.1093/mnras/sty2190)
- Kumamoto, J., Fujii, M. S., & Tanikawa, A. 2019, *MNRAS*, 486, 3942, doi: [10.1093/mnras/stz1068](https://doi.org/10.1093/mnras/stz1068)
- . 2020, arXiv e-prints, arXiv:2001.10690, <https://arxiv.org/abs/2001.10690>
- Lee, H. M. 1995, *MNRAS*, 272, 605, doi: [10.1093/mnras/272.3.605](https://doi.org/10.1093/mnras/272.3.605)
- Loredo, T. J. 2004, *AIP Conf. Proc.*, 735, 195, doi: [10.1063/1.1835214](https://doi.org/10.1063/1.1835214)
- Lousto, C. O., & Zlochower, Y. 2009, *PhRvD*, 79, 064018, doi: [10.1103/PhysRevD.79.064018](https://doi.org/10.1103/PhysRevD.79.064018)
- . 2011, *PhRvL*, 107, 231102, doi: [10.1103/PhysRevLett.107.231102](https://doi.org/10.1103/PhysRevLett.107.231102)
- Lousto, C. O., Zlochower, Y., Dotti, M., & Volonteri, M. 2012, *PhRvD*, 85, 084015, doi: [10.1103/PhysRevD.85.084015](https://doi.org/10.1103/PhysRevD.85.084015)
- Madau, P., & Fragos, T. 2017, *ApJ*, 840, 39, doi: [10.3847/1538-4357/aa6af9](https://doi.org/10.3847/1538-4357/aa6af9)
- Maggiore, M. 2018, *Gravitational Waves: Volume 2: Astrophysics and Cosmology*, Gravitational Waves (Oxford University Press), <https://books.google.it/books?id=3ZNODwAAQBAJ>
- Mandel, I., & de Mink, S. E. 2016, *MNRAS*, 458, 2634, doi: [10.1093/mnras/stw379](https://doi.org/10.1093/mnras/stw379)
- Mandel, I., Farr, W. M., & Gair, J. R. 2019, *MNRAS*, 486, 1086, doi: [10.1093/mnras/stz896](https://doi.org/10.1093/mnras/stz896)
- Mapelli, M. 2016, *MNRAS*, 459, 3432, doi: [10.1093/mnras/stw869](https://doi.org/10.1093/mnras/stw869)
- Mapelli, M., & Giacobbo, N. 2018, *MNRAS*, 479, 4391, doi: [10.1093/mnras/sty1613](https://doi.org/10.1093/mnras/sty1613)
- Mapelli, M., Giacobbo, N., Ripamonti, E., & Spera, M. 2017, *MNRAS*, 472, 2422, doi: [10.1093/mnras/stx2123](https://doi.org/10.1093/mnras/stx2123)
- Mapelli, M., Giacobbo, N., Santoliquido, F., & Artale, M. C. 2019, *MNRAS*, doi: [10.1093/mnras/stz1150](https://doi.org/10.1093/mnras/stz1150)
- Mapelli, M., Hayfield, T., Mayer, L., & Wadsley, J. 2012, *ApJ*, 749, 168, doi: [10.1088/0004-637X/749/2/168](https://doi.org/10.1088/0004-637X/749/2/168)
- Mapelli, M., Spera, M., Montanari, E., et al. 2020, *ApJ*, 888, 76, doi: [10.3847/1538-4357/ab584d](https://doi.org/10.3847/1538-4357/ab584d)
- Marchant, P., Langer, N., Podsiadlowski, P., Tauris, T. M., & Moriya, T. J. 2016, *A&A*, 588, A50, doi: [10.1051/0004-6361/201628133](https://doi.org/10.1051/0004-6361/201628133)
- McKernan, B., Ford, K. E. S., Lyra, W., & Perets, H. B. 2012, *MNRAS*, 425, 460, doi: [10.1111/j.1365-2966.2012.21486.x](https://doi.org/10.1111/j.1365-2966.2012.21486.x)
- McKernan, B., Ford, K. E. S., Bellovary, J., et al. 2018, *ApJ*, 866, 66, doi: [10.3847/1538-4357/aadae5](https://doi.org/10.3847/1538-4357/aadae5)
- Mennekens, N., & Vanbeveren, D. 2014, *A&A*, 564, A134, doi: [10.1051/0004-6361/201322198](https://doi.org/10.1051/0004-6361/201322198)
- Miller, M. C., & Hamilton, D. P. 2002, *MNRAS*, 330, 232, doi: [10.1046/j.1365-8711.2002.05112.x](https://doi.org/10.1046/j.1365-8711.2002.05112.x)
- Miller, M. C., & Lauburg, V. M. 2009, *ApJ*, 692, 917, doi: [10.1088/0004-637X/692/1/917](https://doi.org/10.1088/0004-637X/692/1/917)
- Moody, K., & Sigurdsson, S. 2009, *ApJ*, 690, 1370, doi: [10.1088/0004-637X/690/2/1370](https://doi.org/10.1088/0004-637X/690/2/1370)

- Morscher, M., Pattabiraman, B., Rodriguez, C., Rasio, F. A., & Umbreit, S. 2015, *ApJ*, 800, 9, doi: [10.1088/0004-637X/800/1/9](https://doi.org/10.1088/0004-637X/800/1/9)
- Neijssel, C. J., Vigna-Gómez, A., Stevenson, S., et al. 2019, *MNRAS*, 490, 3740, doi: [10.1093/mnras/stz2840](https://doi.org/10.1093/mnras/stz2840)
- Neumayer, N., Seth, A., & Böker, T. 2020, *A&A Rv*, 28, 4, doi: [10.1007/s00159-020-00125-0](https://doi.org/10.1007/s00159-020-00125-0)
- Nitz, A. H., Dent, T., Davies, G. S., & Harry, I. 2020, arXiv e-prints, arXiv:2004.10015, <https://arxiv.org/abs/2004.10015>
- O’Leary, R. M., Kocsis, B., & Loeb, A. 2009, *MNRAS*, 395, 2127, doi: [10.1111/j.1365-2966.2009.14653.x](https://doi.org/10.1111/j.1365-2966.2009.14653.x)
- Petrovich, C., & Antonini, F. 2017, *ApJ*, 846, 146, doi: [10.3847/1538-4357/aa8628](https://doi.org/10.3847/1538-4357/aa8628)
- Podsiadlowski, P., Langer, N., Poelarends, A. J. T., et al. 2004, *ApJ*, 612, 1044, doi: [10.1086/421713](https://doi.org/10.1086/421713)
- Portegies Zwart, S. F., & McMillan, S. L. W. 2000, *ApJL*, 528, L17, doi: [10.1086/312422](https://doi.org/10.1086/312422)
- Portegies Zwart, S. F., McMillan, S. L. W., & Gieles, M. 2010, *ARA&A*, 48, 431, doi: [10.1146/annurev-astro-081309-130834](https://doi.org/10.1146/annurev-astro-081309-130834)
- Portegies Zwart, S. F., & Yungelson, L. R. 1998, *A&A*, 332, 173
- Qin, Y., Fragos, T., Meynet, G., et al. 2018, *A&A*, 616, A28, doi: [10.1051/0004-6361/201832839](https://doi.org/10.1051/0004-6361/201832839)
- Qin, Y., Marchant, P., Fragos, T., Meynet, G., & Kalogera, V. 2019, *ApJL*, 870, L18, doi: [10.3847/2041-8213/aaf97b](https://doi.org/10.3847/2041-8213/aaf97b)
- Rasskazov, A., & Kocsis, B. 2019, *ApJ*, 881, 20, doi: [10.3847/1538-4357/ab2c74](https://doi.org/10.3847/1538-4357/ab2c74)
- Renzo, M., Farmer, R. J., Justham, S., et al. 2020, *MNRAS*, doi: [10.1093/mnras/staa549](https://doi.org/10.1093/mnras/staa549)
- Rezzolla, L., Barausse, E., Dorband, E. N., et al. 2008, *PhRvD*, 78, 044002, doi: [10.1103/PhysRevD.78.044002](https://doi.org/10.1103/PhysRevD.78.044002)
- Rodriguez, C. L., Amaro-Seoane, P., Chatterjee, S., et al. 2018, *PhRvD*, 98, 123005, doi: [10.1103/PhysRevD.98.123005](https://doi.org/10.1103/PhysRevD.98.123005)
- Rodriguez, C. L., Chatterjee, S., & Rasio, F. A. 2016, *PhRvD*, 93, 084029, doi: [10.1103/PhysRevD.93.084029](https://doi.org/10.1103/PhysRevD.93.084029)
- Rodriguez, C. L., Morscher, M., Pattabiraman, B., et al. 2015, *Physical Review Letters*, 115, 051101, doi: [10.1103/PhysRevLett.115.051101](https://doi.org/10.1103/PhysRevLett.115.051101)
- Rodriguez, C. L., Zevin, M., Amaro-Seoane, P., et al. 2019, arXiv e-prints, arXiv:1906.10260, <https://arxiv.org/abs/1906.10260>
- Samsing, J. 2018, *PhRvD*, 97, 103014, doi: [10.1103/PhysRevD.97.103014](https://doi.org/10.1103/PhysRevD.97.103014)
- Samsing, J., MacLeod, M., & Ramirez-Ruiz, E. 2014, *ApJ*, 784, 71, doi: [10.1088/0004-637X/784/1/71](https://doi.org/10.1088/0004-637X/784/1/71)
- Sana, H., de Mink, S. E., de Koter, A., et al. 2012, *Science*, 337, 444, doi: [10.1126/science.1223344](https://doi.org/10.1126/science.1223344)
- Santoliquido, F., Mapelli, M., Bouffanais, Y., et al. 2020, arXiv e-prints, arXiv:2004.09533, <https://arxiv.org/abs/2004.09533>
- Spera, M., & Mapelli, M. 2017, *MNRAS*, 470, 4739, doi: [10.1093/mnras/stx1576](https://doi.org/10.1093/mnras/stx1576)
- Spera, M., Mapelli, M., Giacobbo, N., et al. 2019, *MNRAS*, 485, 889, doi: [10.1093/mnras/stz359](https://doi.org/10.1093/mnras/stz359)
- Stevenson, S., Berry, C. P. L., & Mandel, I. 2017, ArXiv e-prints, <https://arxiv.org/abs/1703.06873>
- Stone, N. C., Metzger, B. D., & Haiman, Z. 2017, *MNRAS*, 464, 946, doi: [10.1093/mnras/stw2260](https://doi.org/10.1093/mnras/stw2260)
- Tagawa, H., Haiman, Z., & Kocsis, B. 2019, arXiv e-prints, arXiv:1912.08218, <https://arxiv.org/abs/1912.08218>
- Tang, P. N., Eldridge, J. J., Stanway, E. R., & Bray, J. C. 2019, arXiv e-prints, arXiv:1912.04474, <https://arxiv.org/abs/1912.04474>
- Timmes, F. X., Woosley, S. E., & Weaver, T. A. 1996, *ApJ*, 457, 834, doi: [10.1086/176778](https://doi.org/10.1086/176778)
- Tremaine, S. D., Ostriker, J. P., & Spitzer, L., J. 1975, *ApJ*, 196, 407, doi: [10.1086/153422](https://doi.org/10.1086/153422)
- Tutukov, A., & Yungelson, L. 1973, *Nauchnye Informatsii*, 27, 70
- Udall, R., Jani, K., Lange, J., et al. 2019, arXiv e-prints, arXiv:1912.10533, <https://arxiv.org/abs/1912.10533>
- VandenBerg, D. A., Brogaard, K., Leaman, R., & Casagrande, L. 2013, *ApJ*, 775, 134, doi: [10.1088/0004-637X/775/2/134](https://doi.org/10.1088/0004-637X/775/2/134)
- Venumadhav, T., Zackay, B., Roulet, J., Dai, L., & Zaldarriaga, M. 2020, *PhRvD*, 101, 083030, doi: [10.1103/PhysRevD.101.083030](https://doi.org/10.1103/PhysRevD.101.083030)
- Voss, R., & Tauris, T. M. 2003, *MNRAS*, 342, 1169, doi: [10.1046/j.1365-8711.2003.06616.x](https://doi.org/10.1046/j.1365-8711.2003.06616.x)
- Wang, L. 2020, *MNRAS*, 491, 2413, doi: [10.1093/mnras/stz3179](https://doi.org/10.1093/mnras/stz3179)
- Webbink, R. F. 1984, *ApJ*, 277, 355, doi: [10.1086/161701](https://doi.org/10.1086/161701)
- Woosley, S. E. 2017, *ApJ*, 836, 244, doi: [10.3847/1538-4357/836/2/244](https://doi.org/10.3847/1538-4357/836/2/244)
- Yang, Y., Bartos, I., Haiman, Z., et al. 2020, arXiv e-prints, arXiv:2003.08564, <https://arxiv.org/abs/2003.08564>
- . 2019, *ApJ*, 876, 122, doi: [10.3847/1538-4357/ab16e3](https://doi.org/10.3847/1538-4357/ab16e3)
- Zackay, B., Venumadhav, T., Dai, L., Roulet, J., & Zaldarriaga, M. 2019, *PhRvD*, 100, 023007, doi: [10.1103/PhysRevD.100.023007](https://doi.org/10.1103/PhysRevD.100.023007)
- Zevin, M., Samsing, J., Rodriguez, C., Haster, C.-J., & Ramirez-Ruiz, E. 2019, *ApJ*, 871, 91, doi: [10.3847/1538-4357/aaf6ec](https://doi.org/10.3847/1538-4357/aaf6ec)
- Zevin, M., Spera, M., Berry, C. P. L., & Kalogera, V. 2020, arXiv e-prints, arXiv:2006.14573, <https://arxiv.org/abs/2006.14573>

Ziosi, B. M., Mapelli, M., Branchesi, M., & Tormen, G.
2014, MNRAS, 441, 3703, doi: [10.1093/mnras/stu824](https://doi.org/10.1093/mnras/stu824)